THE JOURNAL OF BIOLOGICAL CHEMISTRY VOL. 290, NO. 14, pp. 9222–9238, April 3, 2015

Thiosulfate Dehydrogenase (TsdA) from *Allochromatium vinosum*

*STRUCTURAL AND FUNCTIONAL INSIGHTS INTO THIOSULFATE OXIDATION**

Received for publication, November 3, 2014, and in revised form, February 10, 2015 Published, JBC Papers in Press, February 11, 2015, DOI 10.1074/jbc.M114.623397

José A. Brito[‡1,2], **Kevin Denkmann**[§1], **Inês A. C. Pereira**[‡], **Margarida Archer**[‡3], **and Christiane Dahl**[§4]

From the [‡]*Instituto de Tecnologia Química e Biológica António Xavier, Universidade Nova de Lisboa (ITQB-UNL), Avenida da República, 2780-157 Oeiras, Portugal and the* [§]*Institut für Mikrobiologie & Biotechnologie, Rheinische Friedrich-Wilhelms-Universität Bonn, D-53115 Bonn, Germany*

Background: TsdA oxidizes thiosulfate to tetrathionate and shows unusual histidine-cysteine axial heme coordination.
Results: Characterization of TsdA variants provides various snapshots of both heme environments.
Conclusion: Heme 1 was identified as the catalytic heme along with a substrate binding pocket near Cys^{96}, and a Lys^{208}/Met^{209} ligand switch is observed at heme 2 upon reduction.
Significance: A novel mechanism for thiosulfate oxidation is proposed.

Although the oxidative condensation of two thiosulfate anions to tetrathionate constitutes a well documented and significant part of the natural sulfur cycle, little is known about the enzymes catalyzing this reaction. In the purple sulfur bacterium *Allochromatium vinosum*, the reaction is catalyzed by the periplasmic diheme *c*-type cytochrome thiosulfate dehydrogenase (TsdA). Here, we report the crystal structure of the "as isolated" form of *A. vinosum* TsdA to 1.98 Å resolution and those of several redox states of the enzyme to different resolutions. The protein contains two typical class I *c*-type cytochrome domains wrapped around two hemes axially coordinated by His^{53}/Cys^{96} and His^{164}/Lys^{208}. These domains are very similar, suggesting a gene duplication event during evolution. A ligand switch from Lys^{208} to Met^{209} is observed upon reduction of the enzyme. Cys^{96} is an essential residue for catalysis, with the specific activity of the enzyme being completely abolished in several TsdA-Cys^{96} variants. TsdA-K208N, K208G, and M209G variants were catalytically active in thiosulfate oxidation as well as in tetrathionate reduction, pointing to heme 2 as the electron exit point. In this study, we provide spectroscopic and structural evidence that the TsdA reaction cycle involves the transient presence of heme 1 in the high-spin state caused by movement of the Sγ atom of Cys^{96} out of the iron coordination sphere. Based on the presented data, we draw important conclusions about the enzyme and propose a possible reaction mechanism for TsdA.

Thiosulfate dehydrogenases (TsdAs)[5] catalyze the reversible formation of a sulfur-sulfur bond between the sulfane atoms of two thiosulfate molecules, yielding tetrathionate and releasing two electrons (see Reaction 1) (1). TsdA homologues are widespread among bacteria, agreeing with reports of tetrathionate formation not only by specialized sulfur oxidizers but also by many chemoorganoheterotrophic bacteria (1, 2). In the purple sulfur bacterium *Allochromatium vinosum*, a γ-proteobacterium and member of the Chromatiaceae family (3), thiosulfate is oxidized by two different pathways (4). TsdA catalyzes the one-step oxidation to tetrathionate (Reaction 1), and the Sox system in conjunction with the Dsr system oxidizes thiosulfate completely to sulfate. The degradation of thiosulfate via the Sox/Dsr pathway is initiated by the *c*-type cytochrome SoxXA that catalyzes a reaction closely resembling tetrathionate formation. A sulfur-sulfur bond is formed between the sulfane sulfur of thiosulfate and a cysteine residue present on the SoxYZ substrate carrier protein (Reaction 2) (5–8).

$$^{-}O_3S\text{-}S^{-} + {}^{-}S\text{-}SO_3^{-} + 2\ acc_{ox} \leftrightarrow {}^{-}O_3S\text{-}S\text{-}S\text{-}SO_3^{-} + 2\ acc_{red}$$

$$SoxZY\text{-}S^{-} + {}^{-}S\text{-}SO_3^{-} + 2\ ferricytochrome\ c \rightarrow$$

$$SoxZY\text{-}S\text{-}S\text{-}SO_3^{-} + 2\ ferrocytochrome\ c$$

REACTIONS 1 AND 2

In *A. vinosum*, TsdA is a periplasmic, monomeric 27.2-kDa diheme *c*-type cytochrome. Electronic paramagnetic resonance (EPR) spectroscopy indicated cysteine and methionine as sixth distal axial ligands of the two heme irons. Indeed, Cys^{96} was proven to be essential for catalytic activity (1). At pH 4.0, *Av*TsdA exhibits high specific activity (28,600 units mg^{-1}) with ferricyanide as artificial electron acceptor. On the contrary, the maximum specific activity for the reverse (*i.e.* the tetrathionate-reducing) direction was reported to be very low (22 units

* This work was supported by Deutsche Forschungsgemeinschaft Grant DA 351/7-1; Fundação para a Ciência e a Tecnologia (FCT) Grants PTDC/BBB-BQB/0684/2012, PTDC/BIA-PRO/118535/2010, and PEst-OE/EQB/LA0004/2011; the German Academic Exchange Service; Conselho de Reitores das Universidades Portuguesas; and BioStruct-X (Proposal 1493).
The atomic coordinates and structure factors (codes 4WQ7, 4WQ8, 4WQ9, 4WQA, 4WQB, 4WQC, 4WQD, and 4WQE) have been deposited in the Protein Data Bank (http://wwpdb.org/).
[1] Both authors contributed equally to this work.
[2] Recipient of FCT Fellowship SFRH/BPD/79224/2011.
[3] To whom correspondence may be addressed. Tel.: 351-214-469-747; Fax: 351-214-433-644; E-mail: archer@itqb.unl.pt.
[4] To whom correspondence may be addressed. Tel.: 49-228-73-2119; Fax: 49-228-73-7576; E-mail: ChDahl@uni-bonn.de.

[5] The abbreviations used are: TsdA, thiosulfate dehydrogenase; BisTris, 2-[bis(2-hydroxyethyl)amino]-2-(hydroxymethyl)propane-1,3-diol; r.m.s.d., root mean square deviation; PDB, Protein Data Bank; HiPIP, high-potential iron-sulfur protein.

mg^{-1}). Reduced methylviologen served as artificial electron donor in these *in vitro* assays (2). Taken together, these findings indicate that the *A. vinosum* enzyme is especially adapted to catalyzing thiosulfate oxidation.

In *c*-type cytochromes like TsdA, the heme moieties are covalently bound to the apoprotein via thioether linkages. These are formed by two cysteine residues mostly present in a Cys-*XX*-Cys-His motif (9, 10). The histidine serves as a proximal axial ligand to the iron encapsulated in the porphyrin macrocycle. A few cytochromes show variations of the heme binding motif to $CX_{15}CH$ or even C*XX*CK (11–13). In the C*XX*CK motif, the lysine acts as a proximal heme ligand, such as in the catalytically active site of cytochrome *c* nitrite reductase (14). In six-coordinate *c*-type cytochromes, the distal axial ligand is most commonly a second histidine or a methionine (15). The combination of histidine with other ligands is relatively rare. It includes tyrosine in cytochrome *f* (16), the side chain of lysine in cytochrome *c* nitrite reductase (17) and its physiological partner NrfH (18), asparagine (19) in sphaeroides heme protein (19), and also cysteine. The latter was first discovered in the SoxXA protein of *Rhodovulum sulfidophilum* (20). In the catalytic subunit SoxA, the active site heme-ligating cysteine is modified by a further sulfur atom (*i.e.* it is present as a cysteine persulfide possibly arising from a SoxA-thiocysteine *S*-sulfate intermediate formed during the catalytic cycle) (6, 21). Other examples for His/Cys-ligated hemes in *c*-type cytochromes are the DsrJ protein from *A. vinosum* (22) and *Desulfovibrio desulfuricans* (23), the green heme protein from *Halochromatium salexigens* (24), a triheme cytochrome *c* from *R. sulfidophilum* (25), and the PsbV2 cytochrome from the cyanobacterium *Thermosynechococcus elongatus* (26).

In this work, we crystallized several recombinant forms of *A. vinosum* TsdA and determined the three-dimensional structures of the "as isolated," dithionite-reduced, and tetrathionate-soaked proteins as well as of variants with replacements of putative active site and heme iron-ligating residues. Thereby, we confirmed the proposed axial histidine/cysteine ligation of heme 1 and found a distal axial lysine ligation of the second heme in the oxidized state of the protein. Remarkably, the axial ligand of heme 2 changes to methionine upon reduction, as revealed by several x-ray structures. Assessment of enzymatic activities and electronic absorption properties for wild type TsdA and its variants provided further evidence for unexpected plasticity of heme ligation at both hemes. We identified the substrate-binding site in the vicinity of heme 1, close to Cys^{96} and surrounded by other strictly conserved residues. A catalytic mechanism is herein proposed.

EXPERIMENTAL PROCEDURES

Bacterial Strains, Media, and Growth Conditions—The bacterial strains and plasmids used are described in Table 1. *Escherichia coli* strains were cultivated in NZCYM (27), LB, or 2× YT (28) medium. *E. coli* DH5α was used for molecular cloning.

Recombinant DNA Techniques—All general molecular genetics techniques were described previously (29). Chromosomal DNA of *A. vinosum* was obtained by standard methods as described previously (30). Restriction enzymes, T4 ligase, and *Pfu* DNA polymerase were obtained from Thermo Scientific (Schwerte, Germany) and used according to the manufacturer's instructions. Oligonucleotides for cloning were obtained from Eurofins MWG (Ebersberg, Germany).

Construction of Expression Plasmids and Site-directed Mutagenesis—The *A. vinosum tsdA* gene coding for the mature protein without the signal peptide was amplified and cloned as described earlier (1). Point mutations were introduced into *tsdA* by overlap extension (31) using standard PCR with *Pfu* DNA polymerase (Thermo Scientific) and pPRIBAAvtsdA (1) as the template. For the TsdA-K208G exchange, two fragments were amplified with the following primers: for the first fragment, TsdA_XbaIf and LysGly_rev; for the second fragment, LysGlyfw and IBA1hind_rev. Both fragments were used as templates for amplification of the complete *tsdA* gene carrying the desired point mutation. In this step, TsdA_XbaIfopt and IBA1hind_revopt served as primers. The resulting fragment was restricted with XbaI and HindIII and cloned into pPRIBAAvtsdA, resulting in plasmid pPR-IBAAvtsdAsK208G. The following plasmids were generated applying the same general strategy: pPR-IBAAvtsdAsK208N, pPR-IBAAvtsdAsC96G, pPR-IBAAvtsdAsC96H, and pPR-IBAAvtsdAsC96M (Table 1).

Overproduction, Purification, and Preparation of Recombinant TsdA Wild Type and Mutant Proteins—*E. coli* BL21(DE3) cells containing pPR-IBAAvtsdAs or one of the *tsdA* mutant expression plasmids and pEC86 were cultured in 700 ml of NZCYM medium containing ampicillin (100 mg ml^{-1}) and chloramphenicol (25 mg ml^{-1}) in 1-liter Erlenmeyer flasks at 37 °C and 180 r.p.m. At A_{600} of 0.6, the culture was switched to 25 °C, and the cells were harvested after an additional 16–20 h. Cells were resuspended in 50 mM BisTris-HCl buffer, pH 6.5, and lysed by sonication. After the removal of insoluble cell material by centrifugation (10,000 × *g* for 25 min at 4 °C), TsdA wild type or TsdA mutant proteins were purified by Strep-Tactin affinity chromatography and gel filtration as described before (32).

Protein Techniques—SDS-PAGE was performed as described previously (33). Heme staining in acrylamide gels was done as described (34). Protein concentration of purified protein was determined with the BCA kit from Pierce.

Enzyme Kinetics—Thiosulfate-dependent ferricyanide reduction was measured by following the decrease of absorbance at 420 nm (ϵ = 1.09 mM^{-1} cm^{-1}). 100 mM ammonium acetate buffer (pH 4.0 or 5.0), 1 mM ferricyanide, and varying concentrations of thiosulfate were preincubated in a 0.5-ml cuvette (Hellma Analytics, Mühlheim, Germany) at 30 °C for 5 min. Assays were started by the addition of TsdA, and data were recorded in a Specord 210 spectrophotometer (Analytik Jena, Jena, Germany).

Tetrathionate-dependent methylviologen oxidation was measured by following the decrease of absorbance at 585 nm for the artificial electron donor methylviologen (ϵ = 11.8 mM^{-1} cm^{-1}) prereduced with titanium(III) citrate. The latter was prepared as described by Zehnder and Wuhrmann (35). 100 mM ammonium acetate buffer, pH 5.0, 300 μM titanium(III) citrate-reduced methylviologen and 1 μg of TsdA were preincubated in a 3-ml cuvette (Hellma Analytics) at 30 °C for 5 min. Assays were started by the addition of tetrathionate in varying concentrations, and data were recorded in an Agilent 8453 spectrophotometer (Agilent Technologies, Ratingen, Germany) under anoxic conditions. When necessary, control assays without

TABLE 1
Strains, plasmids, and primers

Strain, primer, or plasmid	Description or sequence	Source
Strains		
E. coli DH5α	*fhuA2 Δ(argF-lacZ)U169 phoA glnV44 Φ80 Δ(lacZ)M15 gyrA96 recA1 relA1 endA1 thi-1 hsdR17*	Ref. 65
E. coli BL21 DE3	*B dcm ompT hsdS($r_B^-m_B^-$) gal*	Novagen
Primers		
tsdAs_f	CCA CAA AGA AA*C ATA TGC* GCG GTG (NdeI)	This work
tsdAs_rev	CCG ACG GGT *GAT ATC* GCG TCG (EcoRV)	This work
TsdA_XbaIfopt	CGG TTT CCC *TCT AGA* AAT AAT (XbaI)	This work
IBA1hind_revopt	GCC GGA TC*A AGC TT*A TTA TTT TTC GAA CT (HindIII)	This work
CysGlyfw	GGC GAT **GGT** TTC GAG	This work
CysGly_rev	CTC GAA **ACC** ATC GCC	This work
CysHisfw	ATC GGC GAT **CAT** TTC GAG	This work
CysHis_rev	CTC GAA **ATG** ATC GCC GAT	This work
CysMetfw	ATC GGC GAT **ATG** TTC GAG CGC	This work
CysMet_rev	GCG CTC GAA **CAT** ATC GCC GAT	This work
LysGlyfw	ATC AAG CAC **GGG** ATG CCG TTA	This work
LysGly_rev	TAA CGG CAT **CCC** GTG CTT GAT	This work
LysAsnfw	ATC AAG CAC **AAC** ATG CCG TTA	This work
MetGly_fw	ATC GGC GAT **ATG** TTC GAG CGC	This work
MetGly_rev	CTAAC GGC **CCC** TTG TGC TT	This work
Plasmids		
pEC86	Cm^r, product from pEC66 and pACYC184 with *E. coli ccmABCDEFGH* genes	Ref. 66
pPR-IBApelB	Ap^r, IBA 1 vector, PelB-leader, Strep-tag, f1 origin,	IBA (Göttingen)
pPR-IBApelBJstrep	Ap^r, PelB-leader, Strep-tag, NcoI-Eco47III fragment of PCR amplified *dsrJ* in pPR-IBApelB	Ref. 22
pPR-IBAAvtsdA	Ap^r, Strep-tag, f1 origin, T7 Promoter, NdeI-EcoRV fragment of PCR amplified *tsdA* in digested pPR-IBApelBJstrep	Ref. 1
pPR-IBAAvtsdAsC_{96}G	Ap^r, C96G mutation introduced into pPRIBAAvtsdA	Ref. 1
pPR-IBAAvtsdAsC_{96}H	Ap^r, C96H mutation introduced into pPRIBAAvtsdA	This work
pPR-IBAAvtsdAsC_{96}M	Ap^r, C96 M mutation introduced into pPRIBAAvtsdA	This work
pPR-IBAAvtsdAsK_{208}G	Ap^r, K208G mutation introduced into pPRIBAAvtsdA	This work
pPR-IBAAvtsdAsK_{208}N	Ap^r, K208N mutation introduced into pPRIBAAvtsdA	This work
pPR-IBAAvtsdAsM_{209}G	Ap^r, M209G mutation introduced into pPRIBAAvtsdA	This work

enzyme were run to calculate the chemical oxidation of methylviologen by tetrathionate.

Spectroscopic Methods—UV-visible spectra were recorded in a Specord 210 spectrophotometer (Analytik Jena) and processed with Microsoft Excel.

Crystallization and Data Collection—TsdA crystallization has been reported previously (32). In summary, TsdA at a concentration of 8 mg ml^{-1} in 20 mM BisTris-HCl, pH 6.5, crystallized in a condition comprising 23.5% (w/v) PEG 3350, 0.2 M $(NH_4)_2SO_4$, 0.1 M BisTris, pH 6.28, and 0.1 M NaI (as additive). 3-μl drops were set up in an Oryx 6 dispensing robot (Douglas Instruments), using an MRC Maxi 48-well crystallization plate (Swissci), by mixing 1.2 μl of protein solution with 1.5 μl of precipitant and 0.3 μl of additive, and equilibrated against a reservoir of 120 μl of crystallization condition. TsdA mutants and TsdA incubated with ligands crystallized in similar conditions as the "as isolated" protein. Other TsdA variants were obtained by soaking the WT crystals with an excess of ligands (thiosulfate, tetrathionate, and bisulfite) or reduced with dithionite as described in Table 3. Crystals were then back-soaked with the cryoprotection solution. For cryoprotection, crystals were transferred to a new drop with higher PEG 3350 concentration (25.4% w/v) supplemented with 5% (v/v) PEG 400. Complete x-ray diffraction data sets were collected at several synchrotrons (see Table 2 for details).

Data were indexed, integrated, and scaled using *XDS* and converted to MTZ format with *XDSCONV* (36). R_{free} flags for all data sets were created at this stage corresponding to 5% of the measured reflections for each data set. For phasing, a data set was collected at a wavelength of 1.722 to 1.98 Å resolution with an overall R_{merge} of 7.2 and 87% completeness (Table 2) on the XALOC beamline at the ALBA synchrotron (Barcelona, Spain).

Structure Determination and Refinement—The AutoSol wizard in *PHENIX* (37) was used to determine the phases by the single anomalous dispersion method, making use of the anomalous scattering properties of the heme irons. *phenix.xtriage* was used to assess the extent of the anomalous signal that was present to 2.6 Å resolution. A search for two iron atoms yielded one single solution with five sites (corresponding to two fully occupied heme iron atoms and three partially occupied iodides), yielding a Bayes correlation coefficient of 36.6% for map skew and a figure of merit of 37.9%. The electron density map was not readily interpretable and was subjected to one round of thorough density modification with the program *RESOLVE* (38) as implemented in *PHENIX* (39). The map was significantly improved, allowing the recognition of the heme prosthetic groups and secondary structure elements, yielding a correlation for local r.m.s.d. electron density of 77%. The AutoBuild wizard in *PHENIX* was used for automated model building and was able to build 182 residues out of 252 (full construct), with 148 docked to sequence with a map-model correlation coefficient of 45%. Iterative manual model building and refinement were carried out in a cyclic manner with *COOT* (40) and *phenix.refine* (41) until a complete model was built and refinement convergence was achieved (Table 2).

The Ramachandran diagram was plotted with *RAMPAGE* (42), and the model was validated with *MolProbity* (43), as implemented in *PHENIX*.

Because all TsdA crystals were isomorphous, the remaining structures of TsdA variants were determined by an initial rigid body refinement with *BUSTER-TNT* (44). The heme prosthetic groups as well as the coordinating residues were removed from the model used in this refinement, and the program macro "Missing Atoms," together with the "-L" flag ("presence of an

TABLE 2
Data collection and refinement statistics for TsdA structures

	"As isolated"	Tetrathionate soak	Dithionite soak	Tetrathionate co-crystal	Bisulfite soak	K208N mutant	K208G mutant (I)	K208G mutant (II)
PDB code	4WQ7	4WQ8	4WQ9	4WQA	4WQB	4WQC	4WQD	4WQE
Data collection								
Synchrotron	ALBA	PETRA III	PETRA III	ESRF	SLS	Diamond	Diamond	ESRF
Beamline	XALOC	P14	P14	ID29	X06DA	I02	I02	ID29
Wavelength (Å)	1.722	1.239	1.239	0.999	1.000	0.954	0.954	0.976
Resolution range (Å)[a]	44.81–1.98 (2.06–1.98)	39.42–1.40 (1.45–1.40)	34.93–1.47 (1.52–1.47)	46.48–1.64 (1.70–1.64)	28.70–1.50 (1.56–1.50)	39.44–1.56 (1.62–1.56)	39.45–1.22 (1.27–1.22)	35.33–1.40 (1.45–1.40)
Space group	C 1 2 1	C 1 2 1	C 1 2 1	C 1 2 1	C 1 2 1	C 1 2 1	C 1 2 1	C 1 2 1
Unit cell								
a, *b*, *c* (Å)	79.21, 69.88, 57.86	79.03, 70.13, 57.72	79.29, 69.86, 57.81	79.19, 71.05, 57.78	79.26, 70.73, 57.85	79.05, 71.03, 57.81	79.09, 70.81, 57.87	79.27, 70.66, 57.95
α, β, γ (degrees)	90, 129.25, 90	90, 129.20, 90	90, 129.42, 90	90, 129.11, 90	90, 129.25, 90	90, 129.10, 90	90, 128.99, 90	90, 129.35, 90
Total no. of reflections	52,513 (4004)	135,817 (6521)	123,413 (9454)	98,872 (7844)	129,344 (11,946)	77,483 (6826)	153,728 (13,931)	170,468 (10,020)
No. of unique reflections	29,056 (2310)	39,950 (2012)	38,853 (3507)	29,735 (2803)	37,651 (3578)	33,997 (3162)	68,883 (6644)	43,439 (1538)
Multiplicity	1.8 (1.7)	3.4 (3.2)	3.2 (2.7)	3.3 (2.8)	3.4 (3.3)	2.3 (2.2)	2.2 (2.1)	3.9 (3.8)
Completeness (%)	87 (70)	81 (42)	93 (86)	97 (92)	95 (91)	96 (90)	94 (91)	81 (56)
Mean I/σ(I)	9.50 (3.76)	13.68 (2.21)	9.01 (1.93)	11.03 (1.99)	24.42 (7.27)	11.12 (1.42)	13.40 (2.28)	13.35 (1.82)
R_{merge} (%)[b]	7.2 (28.1)	7.7 (55.9)	9.2 (53.8)	6.8 (49.9)	2.8 (15.2)	5.4 (50.3)	3.5 (40.3)	6.2 (99.4)
CC* (%)[c]	99.8 (96.8)	99.7 (89.6)	99.6 (89.9)	100 (95.6)	1 (99.6)	1 (94.1)	1 (95.9)	99.9 (69.4)
Refinement								
R_{cryst} (%)[d]	13.8	13.8	14.0	16.5	12.2	14.6	15.1	13.8
R_{free} (%)[e]	19.3	16.5	17.9	20.4	14.7	20.1	18.3	17.0
No. of atoms								
Protein	1727	1771	1749	1719	1730	1763	1757	*1726*
Ligands	94	136	103	100	110	104	100	*101*
Waters	164	226	234	207	245	247	257	*220*
r.m.s.d. bonds (Å)	0.012	0.010	0.015	0.011	0.009	0.010	0.010	0.010
r.m.s.d. angles (degrees)	1.58	1.60	1.51	1.60	1.48	1.48	1.49	1.49
Protein residues	Thr^5-Pro^{210} Ser^{216}-Phe^{237}	Thr^5-Met^{209} Leu^{217}-Phe^{237}	Thr^5-Gly^{212} Ser^{216}-Phe^{237}	Thr^5-Met^{209} Ser^{216}-Phe^{237}	Thr^5-Gly^{212} Ser^{216}-Phe^{237}	Thr^5-Leu^{211} Ser^{216}-Phe^{237}	Thr^5-Met^{209} Ser^{216}-Phe^{237}	Thr^5-Met^{209} Ser^{216}-Phe^{237}
Ramachandran plot								
Most favored (%)	98	98	98	97	98	98	97	97
Allowed (%)	2	2	2	3	2	2	3	3
Outliers (%)	0	0	0	0	0	0	0	0
B-Factors (Å^2)								
Protein	21.27	19.40	16.25	25.28	22.71	25.02	20.05	13.94
Ligands/ions	17.42	15.32	14.69	20.92	21.18	24.87	15.88	10.14
Waters	30.22	30.55	29.21	34.29	34.48	35.31	30.58	25.51

[a] Information in parenthesis refers to the last resolution shell.
[b] $R_{merge} = \Sigma_h\Sigma_l|I_{hl} - \langle I_h\rangle|/\Sigma_h\Sigma_l\langle I_h\rangle$, where I_{hl} is the Ith observation of reflection h and $\langle I_h\rangle$.
[c] CC* as described by Karplus and Diederichs (67).
[d] $R_{cryst} = \Sigma_h||F_{obs(h)}| - |F_{cal(h)}||/\Sigma_h|F_{obs(h)}|$, where $F_{obs(H)} - F_{cal(h)}$ are the observed and calculated structure factors for reflection h, respectively.
[e] R_{free} was calculated the same way as R_{factor} but using only 5% of the reflections, which were selected randomly and omitted from refinement.

unknown ligand" in *BUSTER-TNT*), was used to render clear electron density in those regions. Cycles of manual model building were intercalated with crystallographic refinements until convergence (Table 2), as described above. All figures were rendered with PyMOL (45).

RESULTS

Crystallization and Structure Determination—The crystal structure of recombinant TsdA from *A. vinosum* was solved by iron-single anomalous dispersion. Crystals belong to the monoclinic space *C*2, with unit cell parameters $a = 79.2$, $b = 69.9$, $c = 57.9$ Å, $\beta = 129.3°$. The crystal structure contains one monomer in the asymmetric unit, corresponding to a Matthews coefficient (46) of 2.31 Å^3 Da^{-1} and a solvent content around 47%. The "as isolated" structure was refined to 1.98 Å with a R_{cryst} of 13.8% and R_{free} of 19.3%. The model comprises residues Thr^5–Pro^{210} and Ser^{216}–Phe^{237}, two heme molecules, three iodide ions, one sulfate, and 164 water molecules. In this work, we numbered TsdA residues without integrating the 27-amino acid signal peptide that is removed during transport of the protein into the periplasm (1) (*i.e.* only the residues present in the mature protein are numbered). The electron density maps are generally of good quality, except for a disordered loop between Leu^{211} and Asp^{215} and the N- and C-terminal amino acid residues (4 and 15 residues, respectively).

As pointed out previously (32), using NaI as an additive was absolutely crucial to obtain single, good diffraction quality crystals for data collection. Structural analysis shows one iodide in a hydrophobic pocket formed by Pro^{186}, Pro^{233}, and Pro^{235}. The presence of this ion at this position helps to stabilize the interactions that occur with a symmetry-related molecule, namely with residues Pro^{11}, Ala^{12}/Ala^{13}/Ala^{14}, Leu^{15}/Leu^{16}, and Pro^{17}. Interestingly, the maps show some disorder in this region with evidence for an alternate conformation of the main chain around Pro^{17}. Remarkably, a second iodide ion is located near the cysteine coordinating heme 1 and within 4 Å distance to the side chains of Cys^{96}, Arg^{82}, Arg^{92}, and Ser^{100}, the backbone of Gly^{194}, and two water molecules. The third iodide is found nested between the side chains of Leu^{39}, Pro^{40}, and Phe^{42} and is only observed in the "as isolated" structure. Final model parameters and relevant statistics for all TsdA structures characterized are shown in Table 2.

Overall Fold of TsdA and Similar Structures—TsdA is a heart-shaped molecule with approximate overall dimensions $35 \times 45 \times 55$ Å^3. The molecule is organized in two domains related by a pseudo-2-fold symmetry axis, each one displaying

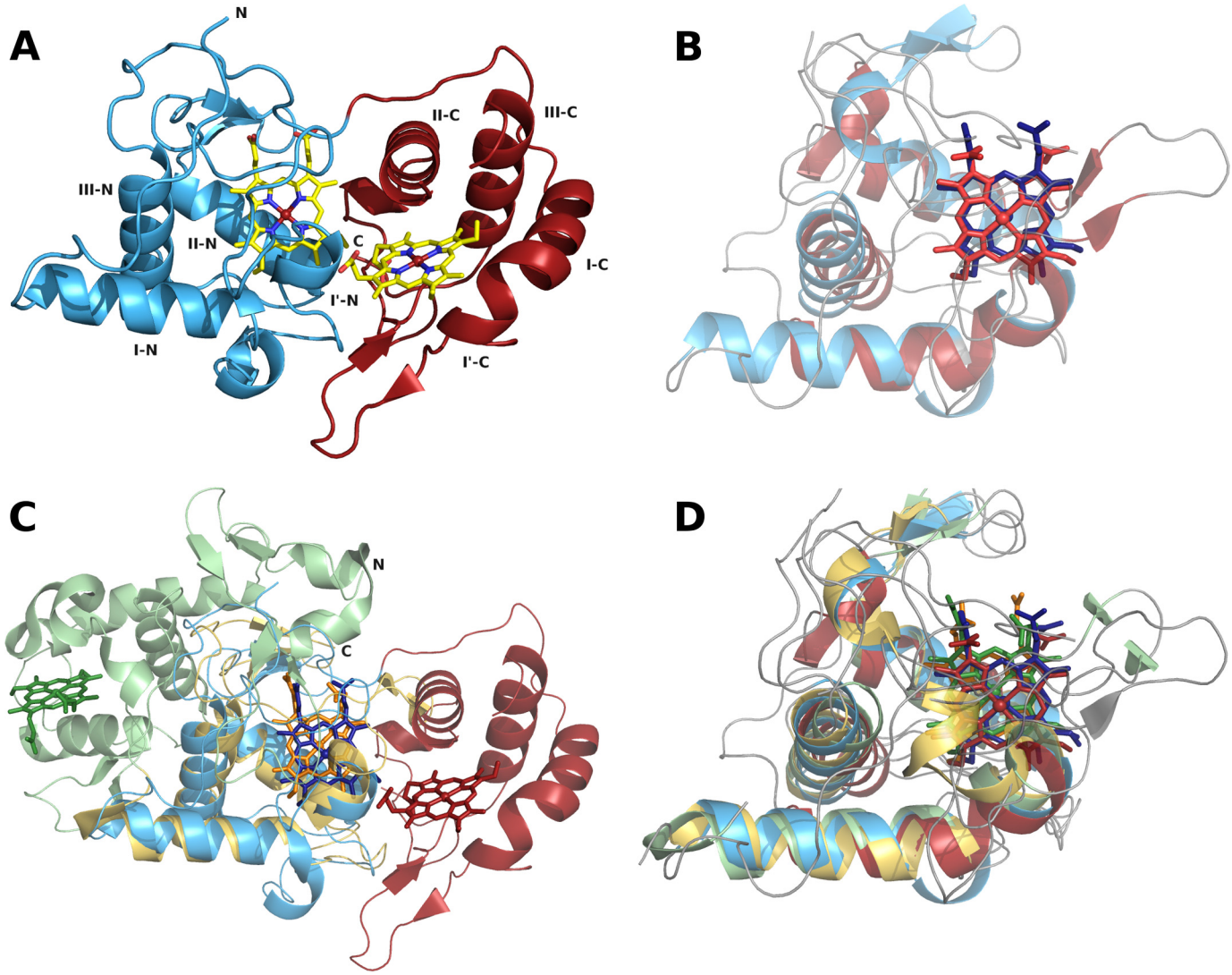

FIGURE 1. **TsdA structure and comparison with SoxA.** *A*, TsdA overall fold with N-terminal domain (residues 5–138) represented in *blue* and C-terminal domain (residues 139–237) in *red*; the heme prosthetic groups are *colored* by atom type (*yellow* for carbon, *blue* for nitrogen, *red* for oxygen, and *dark red* for iron; this *color code* will be used in all figures). *B*, TsdA domains (*colored* as in *A*), superposed with the heme groups displayed in the *same colors* as their corresponding domains (heme 1 in *blue* and heme 2 in *red*). *C*, structural superposition of *A. vinosum* TsdA with *R. sulfidophilum* SoxA, for which the N-terminal domain (residues 51–150) is shown in *green* (corresponding heme group in *dark green*), and the C-terminal domain (residues 151–250) is shown in *yellow* (corresponding heme group in *orange*). *D*, structural superposition of *A. vinosum* TsdA with *R. sulfidophilum* SoxA individual domains (*color code* as in *B* and *C*).

the typical class I *c*-type cytochrome topology (Fig. 1*A*). Each domain harbors four α helices (residues 20–23 (I_N), 49–51 (I'_N), 89–98 (II_N), and 111–123 (III_N)) in the N terminus and four α helices (149–159 (I_C), 161–164 (I'_C), 198–208 (II_C), and 219–229 (III_C)) in the C terminus that surround each heme molecule (Fig. 1*B*). The two domains superimpose with an r.m.s.d. of 2.5 Å with 66 structurally aligned residues that correspond to only 16.7% of sequence identity. Helices $I_{N/C}$ and $III_{N/C}$ intersect almost perpendicularly with each other, whereas helices $I_{N/C}$ and $II_{N/C}$ reside on opposite sides of the heme plane (Fig. 1*A*). Interestingly, there is an insertion of 14 amino acids (residues 35–48), between helices I_N and I'_N corresponding to an extra α-helix in the N-terminal domain that is not present in the C-terminal domain. Each domain has an anti-parallel two-stranded β-sheet, but these do not superimpose with each other, being located in opposite sides of the heme plane. In summary, these observations suggest that TsdA resulted from a gene duplication event.

TsdA coordinates were submitted to the DALI server (47), the highest match being with the SoxA subunit of *R. sulfidophilum* SoxAX complex (PDB entry 1H31), with a *Z*-score of 12.0 and r.m.s.d. of 2.5 Å, corresponding to 102 aligned Cα atoms and 22% sequence identity. Interestingly, the two superimposed domains correspond to the N-terminal domain of TsdA with the C-terminal domain of the SoxA subunit (Fig. 1*C*). Heme 1 of TsdA superimposes well with heme 2 of the SoxA subunit, both displaying the typical saddle distortion common in *c*-type cytochromes. Similar to TsdA, SoxAX also displays a pseudo-2-fold symmetry axis relating the two heme domains, as discussed previously (6, 21), but this domain arrangement differs from that of TsdA (Fig. 1*C*). Fig. 1*D* highlights the pseudo-2-fold symmetry of both TsdA and SoxA protein structures. TsdA also superimposes with other cytochromes, like the C-terminal domain of cbb_3 oxidase subunit III from *Pseudomonas stutzeri* (PDB entry 3MK7), cytochrome c_6 from the brown alga *Hizikia fusiformis* (PBD entry 2ZBO), and cytochrome c_6

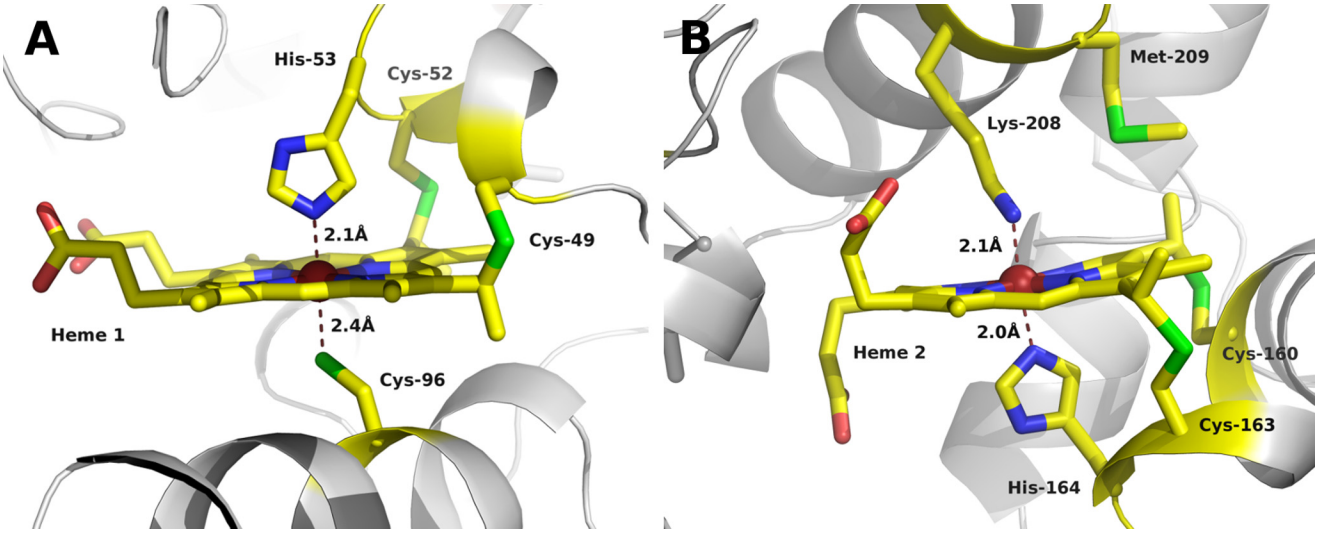

FIGURE 2. **Heme coordination of "as isolated" TsdA (PDB code 4QW7).** *A*, heme 1 is coordinated by His^{53} and Cys^{96}. *B*, heme 2 is coordinated by His^{164} and Lys^{208}. A schematic representation is shown in *pale gray* with heme moieties and coordinating amino acid residues shown in *sticks* (*color code* as in Fig. 1 with sulfur atoms in *green*).

TABLE 3
TsdA heme coordination and vicinity

X-ray model	PDB code	Conditions	Heme 1 coordination (occupancy)[a]	Heme 1 vicinity (occupancy)[a]	Heme 2 coordination (occupancy)[a]
"As isolated"	4WQ7		His^{53}/Cys^{96}	I^- (0.56)	His^{164}/Lys^{208}
Tetrathionate soak	4WQ8	Crystal soaked for 6 h in crystallization solution supplemented with 5 mM tetrathionate	His^{53}/Cys^{96}-S (0.41) His^{53}/Cys^{96}-O2 (0.59)		His^{164}/Lys^{208}
Dithionite soak	4WQ9	Crystal soaked for a few min in crystallization solution supplemented with 1 M dithionite	His^{53}/Cys^{96} (0.42) His^{53}/Cys^{96}-O2 (0.58) $His^{53}/H_2S/S^{2-}$ (0.77)	$S_2O_3^{2-}$ (0.42)	His^{164}/Met^{209}
Tetrathionate co-crystal	4WQA	Crystal obtained after the incubation of TsdA with 5× molar excess of tetrathionate	His^{53}/Cys^{96}-S	$S_2O_3^{2-}$ (0.56) H_2O	His^{164}/Lys^{208}
Bisulfite soak	4WQB	Crystal soaked for a few min in a 37% (w/v) sodium bisulfite solution	His^{53}/Cys^{96}-S	$S_2O_3^{2-}$ (0.75) H_2O	His^{164}/Met^{209}
K208N mutant	4WQC		His^{53}/Cys^{96} (0.64) His^{53}/Cys^{96} (0.36)	$S_2O_3^{2-}$ (0.75)	His^{164}/Met^{209}
K208G mutant (I)	4WQD		His^{53}/Cys^{96}-S (0.40) His^{53}/Cys^{96} (0.60)		His^{164}/Met^{209} (0.43) His^{164}/Met^{209} (0.57)
K208G mutant (II)	4WQE		His^{53}/Cys^{96}-S	$S_2O_3^{2-}$ (0.61) $S_2O_3^{2-}$ (0.50) H_2O	His^{164}/Met^{209}

[a] The occupancy is 1 unless otherwise stated.

from the *Phaeodactylum tricornutum* (PDB entry 3DMI), which are the next closest hits. These proteins display *Z*-scores of 8.6 (cbb_3 oxidase), and 8.5 (both cytochromes c_6), for 77, 74, and 75 structurally aligned Cα atoms, respectively. Sequence identities range from 23 to 31%, and superposition occurs with the C-terminal domain of TsdA, not with its N terminus as with SoxA.

Heme Coordination in Oxidized TsdA—The structure of the "as isolated" oxidized TsdA shows that the two heme groups are covalently bound to the polypeptide chain through the thioether bonds of Cys^{49} and Cys^{52} for heme 1 and Cys^{160} and Cys^{163} for heme 2. The heme 1 iron is hexacoordinated with His^{53} as the proximal axial ligand and Cys^{96} as the distal one, as proposed previously (1) (Fig. 2*A* and Table 3). Remarkably, heme 2 iron is axially coordinated by His^{164} and Lys^{208} (Fig. 2*B* and Table 3). This coordination was quite unexpected because this lysine residue is not conserved in other thiosulfate dehydrogenase proteins. Instead, an asparagine residue is usually located at the equivalent position, followed by a strictly conserved methionine (Met^{209} in *A. vinosum* TsdA) (1).

The Fe-Fe distance between the two hemes is around 15.5 Å, with the closest atomic distance being 4.7 Å. This is close to the range seen in other two-domain cytochrome *c* proteins. For hemes at a distance of <14 Å, electron transfer has been reported to be rapid and essentially independent of the environment between the hemes (48). The two hemes form a diheme perpendicular stacked arrangement, a typical motif in multiheme cytochromes (49). Furthermore, both TsdA hemes are quite solvent-exposed with positive electrostatic potential around the cleft (see below; Fig. 3). Together, these findings confirm that heme 1 and heme 2 constitute a redox-linked pair with facile electron flow between them.

Structural Properties of Heme 1—Several three-dimensional structures of TsdA were obtained, in different redox states and complexed with ligands, as well as structures of several TsdA variants (see below). The heme coordinations in these structures are summarized in Table 3. The PDB codes mentioned below refer to this table.

Comparison of the characterized structures revealed substantial conformational and chemical heterogeneity around Cys^{96}, the distal ligand of heme 1, which is in agreement with previous EPR data (1). We found that in some TsdA structures (*e.g.* in the TsdA-K208N structure shown in Fig. 4*A*) (PDB entry

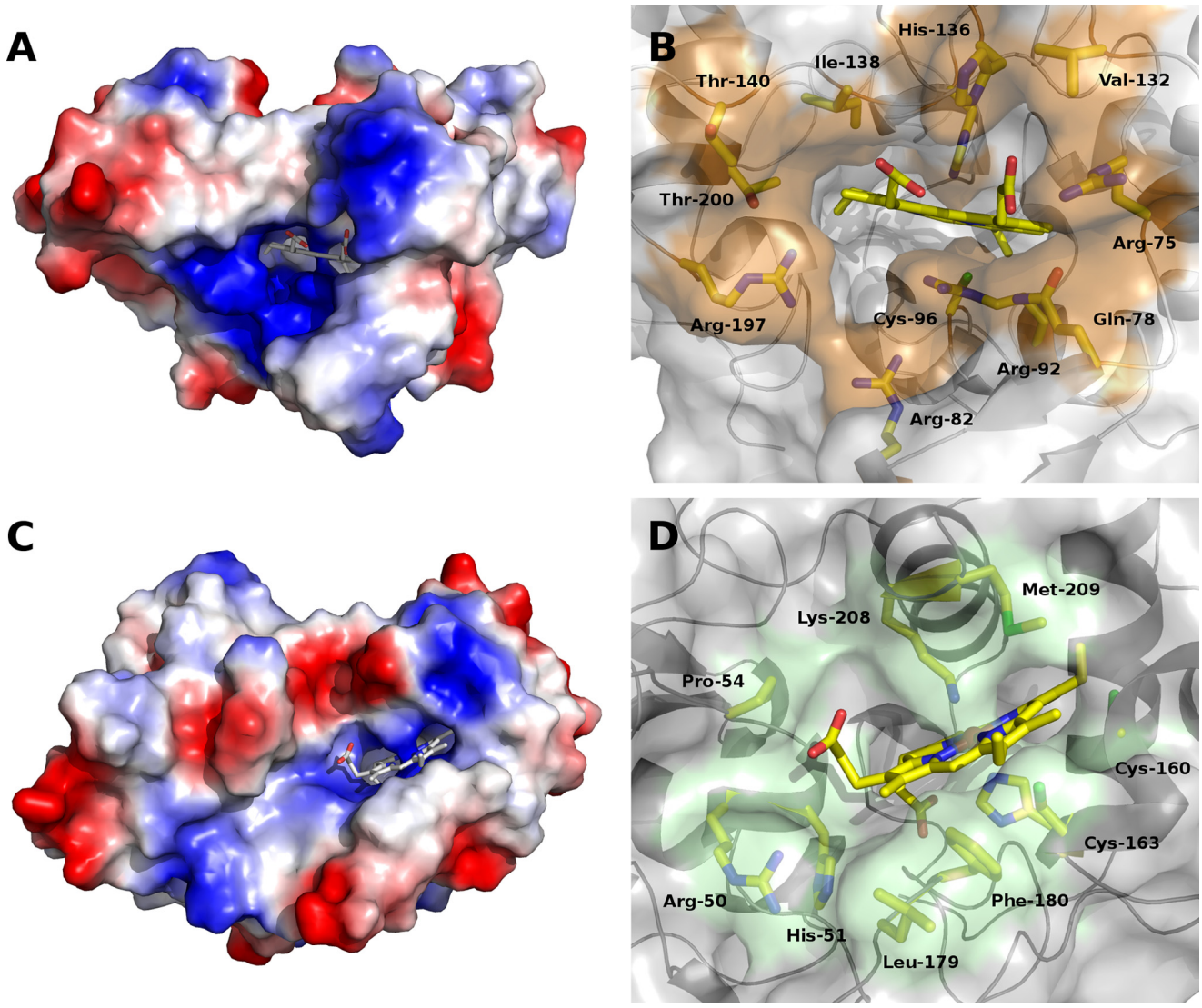

FIGURE 3. **TsdA heme environments.** *A* and *C*, TsdA electrostatic surface potential highlighting the exposure of hemes 1 and 2, respectively. *B* and *D*, *enlarged view* of hemes 1 and 2, respectively; the amino acid residues forming the cleft's entrance are *labeled*.

4WQC; Table 3), this residue is present in two different conformations. In the main conformation, Cys^{96} is directly coordinating the iron through its Sγ, whereas in the minor conformer, this Sγ is tilted away by ~50° from the heme-coordinating position and is no longer bound to the iron. The movement of the sulfur is due solely to rotation of the cysteine Cα-Cβ bond and does not involve any major backbone rearrangements.

In several structures, Cys^{96} is in a persulfurated state, similar to what has been observed previously in the crystal structure of SoxA (6, 7, 50). The persulfuration is complete, for example, in the structure where the protein was co-crystallized with tetrathionate (PDB 4WQA) or from a crystal soaked with sodium bisulfite (Fig. 4*B*, PDB entry 4WQB). However, in some cases, the persulfuration of Cys^{96} is only partial (*e.g.* in one of the two TsdA-K208G structures characterized) (PDB entry 4WQD). Moreover, when the protein is isolated and crystallized in the presence of tris(2-carboxyethyl)phosphine, the persulfuration is not observed (data not shown).

Further heterogeneity was detected for Cys^{96} as in some structures it is present in a double oxidized sulfinate state (Table 3). The Cys^{96} sulfinate state probably results from oxidative damage during the long crystallization process at room temperature, as also observed in other enzymes (51). In the tetrathionate-soaked crystal, the partially persulfurated cysteine is also oxidized to the sulfinate state (PDB entry 4WQ8), whereas in the dithionite-reduced crystal, Cys^{96} is found in two different states, either as a sulfinate or as the unmodified cysteine, and a sulfide was modeled coordinating the heme, which is not bound to Cys^{96} (Fig. 4*C*, PDB entry 4WQ9). This interpretation is based on the shape and contour of the electron density maps, its biochemical plausibility, and refinement results. The presence of a reductant (dithionite) in aerobic conditions leads to generation of reactive oxygen species that are particularly damaging and may produce the sulfinate. On the other hand, if the sulfinate state was already present before dithionite treatment, it will not be reduced because sulfinate is in an irreversible oxidation state. The sulfide ion coordinating the heme in the dithionite-reduced structure (PDB entry 4WQ9) induces a third conformation for Cys^{96} (Fig. 4*C*). This sulfide most likely originates from

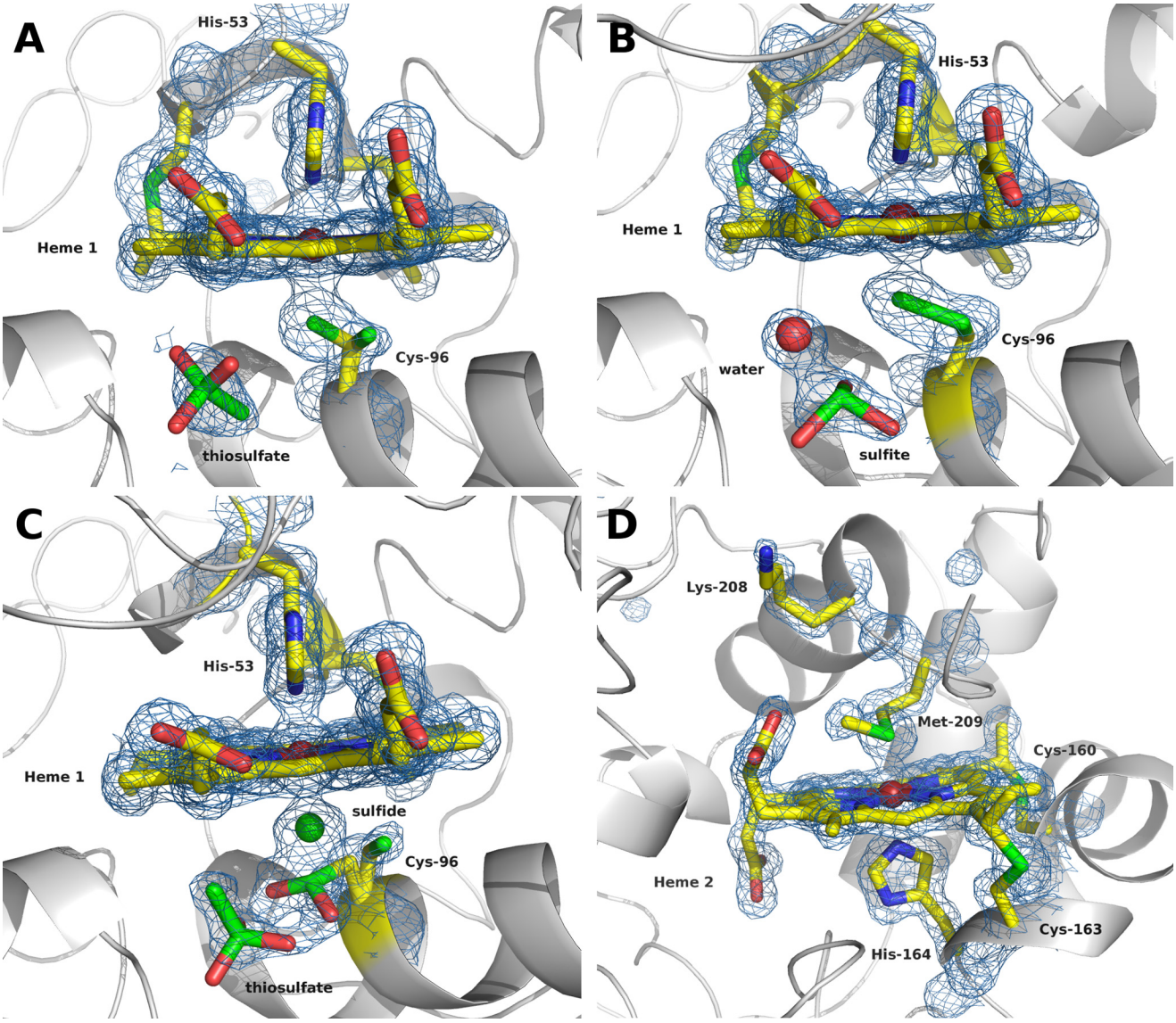

FIGURE 4. **Vicinity of heme 1 distal side and ligand switch at heme 2.** $2mF_o - DF_c$ electron density map contoured at 1σ level around heme 1 in TsdA-K208N variant showing an alternate conformation for Cys^{96} and a thiosulfate (PDB code 4QWC) (*A*), and heme 1 from a bisulfite-soaked crystal displaying a persulfurated cysteine, a sulfite, and water molecule (PDB code 4QWB) (*B*). *C*, heme 1 from a dithionite-soaked crystal showing a Cys^{96} double conformation, one of which is in a sulfinate form, a thiosulfate and a sulfide ion coordinating the heme (PDB code 4QW9). *D*, heme 2 from a dithionite-soaked crystal revealing a ligand switch upon reduction; Lys^{208} moves toward the interior of the protein, whereas Met^{209} coordinates heme 2 (PDB code 4QW9).

dithionite, which is known to usually contain a mixture of sulfur compounds.

Close to heme 1, near Cys^{96}, a conspicuous cleft is present that is lined by Arg^{82}, Arg^{92}, and Arg^{197}, which lie on the same side of the heme, with Arg^{197} closer to the cleft's entrance (Fig. 3*B*). Arg^{197} is not strictly conserved but is replaced by serine in some TsdA sequences (1). This basic cleft is readily solvent-accessible, providing access to Cys^{96} and heme 1. It is noteworthy that the side chain of strictly conserved Arg^{92} is only 3.6 Å away from the Sγ of Cys^{96} and is also close to Arg^{82}. A positive charge appears to be important at the latter position because sequence comparisons reveal conservation of either arginine or lysine (1). Because Cys^{96} is essential for TsdA catalytic activity (1), we propose that this positive groove is the ligand binding pocket that provides access of thiosulfate to the active site. A very similar cluster of basic residues has been found in the SoxA structure and was also suggested to be the active site channel for anionic substrates (6).

In some structures, the anomalous difference map showed a strong blob of electron density (above 5σ contour) inside this active site cavity and close by Cys^{96}. This extra density was modeled as an iodide ion (from the crystallization buffer), and the refinement outcome was reasonable. Soaking crystals of wild type protein with thiosulfate was not successful in providing a structure with substrate bound to the active site, most likely because the high solvent accessibility is linked to a low residence time of bound substrate. However, a partially occupied thiosulfate is observed in three TsdA structures (Table 3): that of the K208N variant (Fig. 4*A*, PDB entry 4WQC), one of the K208G variants (Fig. 5*C*, PDB entry 4WQE), and the dithionite-reduced wild type protein (Fig. *4C*, PDB entry 4WQ9). In all three cases, the thiosulfate is stabilized by hydrogen bonds to

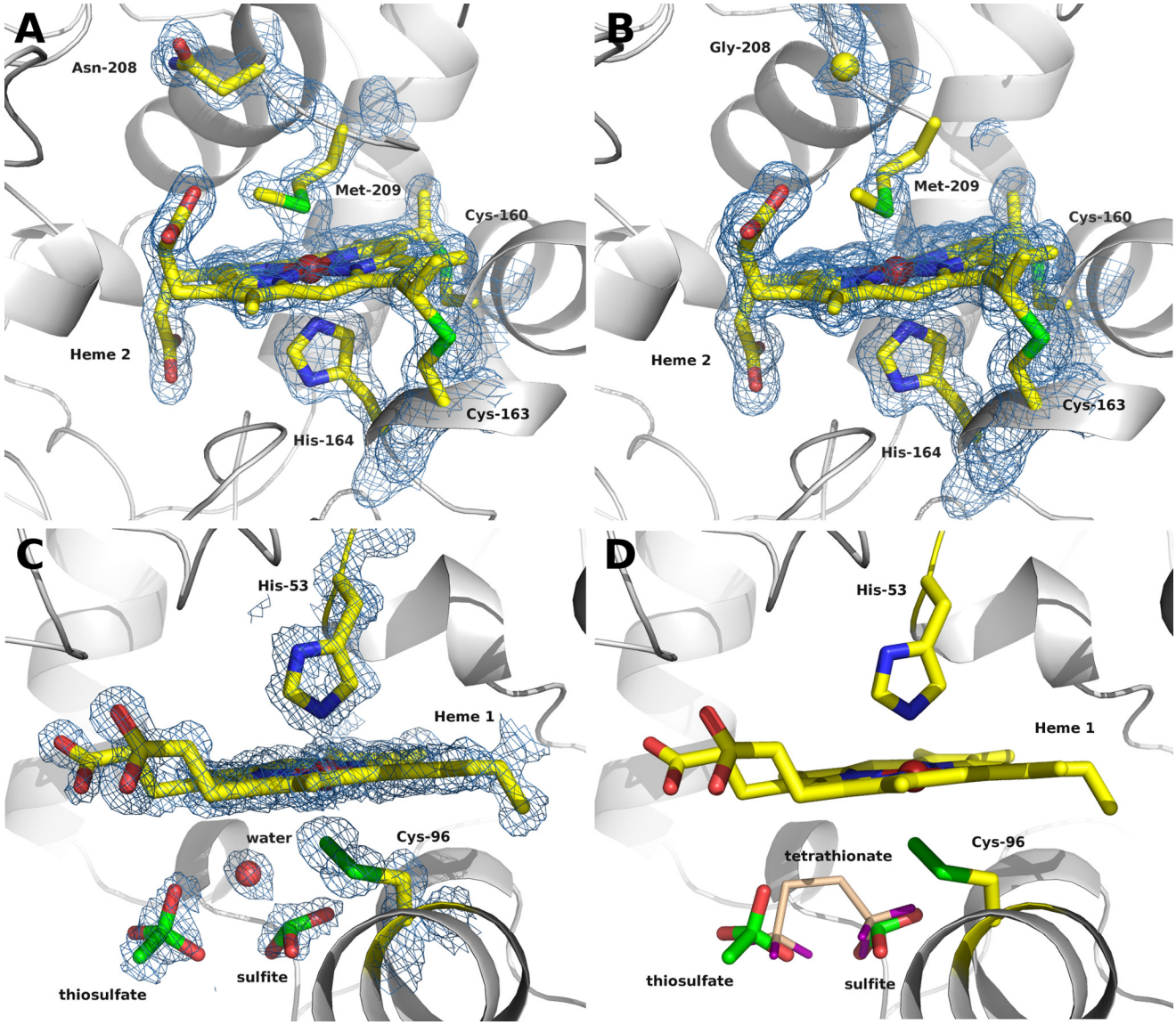

FIGURE 5. **Heme coordination of TsdA variants.** $2mF_o - DF_c$ electron density map contoured at 1.5σ level around heme 2 in TsdA-K208N (PDB code 4WQC) (*A*), heme 2 in TsdA-K208G (PDB code 4WQE) (*B*), and heme 1 in TsdA-K208G (PDB code 4WQE) (*C*) with a thiosulfate, sulfite, and water molecule. *D*, same representation as in *C* with a modeled tetrathionate ion, represented in *thinner sticks*, based on the spatial arrangement of the other observed ions.

Arg^{82}, Arg^{92}, and/or Ser^{100}. Arg^{92} is a strictly conserved residue, Arg^{82} is conservatively substituted by Lys in some TsdAs (and in SoxA), and Ser^{100} is strictly conserved among TsdAs and is replaced by Thr in SoxA (1).

In the TsdA-K208N structure (PDB entry 4WQC), the thiosulfate molecule was modeled with 75% occupancy (Fig. 4*A*). In this structure, the S1–S2 bond of thiosulfate points toward helix II_N (where Cys^{96} lies), and the oxygen atoms are closer to the heme. The Sγ of Cys^{96} was modeled in two alternate conformations, as described above. The iron-coordinating Sγ is 3.6 Å away from S2 and 4.2 Å from the closest oxygen atom of $S_2O_3^{2-}$. In the dithionite-reduced structure (PDB entry 4WQ9), the S1–S2 bond of thiosulfate points toward the heme (Fig. 4*C*). This thiosulfate conformation is rotated by almost 180° relative to that in the TsdA-K208N (Fig. 4*A*). We consider this conformation where the thiosulfate S1–S2 bond points toward the heme the more likely physiological position for the substrate (see below).

It is interesting to note that in the three structures where full persulfuration of Cys^{96} is observed (TsdA-tetrathionate co-crystal, bisulfite soak, and K208G variant II; Table 3), a sulfite molecule is present at the basic cleft instead of thiosulfate and is in the same spatial position as the sulfonate group of the thiosulfate molecule in the dithionite-reduced structure. Moreover, the position of the S1 atom of thiosulfate is occupied in these structures by a water molecule. Therefore, the geometry and spatial arrangement of the sulfite and the water molecule resemble a thiosulfate molecule (Figs. 4*B* (PDB entry 4WQB) and 5*C* (PDB entry 4WQE)). Here, the water oxygen is at a distance of 3.8 and 5.4 Å from the Cys^{96} Sγ and Sδ atoms, respectively. The amino acid residues stabilizing the sulfite are identical to those stabilizing thiosulfate. Furthermore, in TsdA-

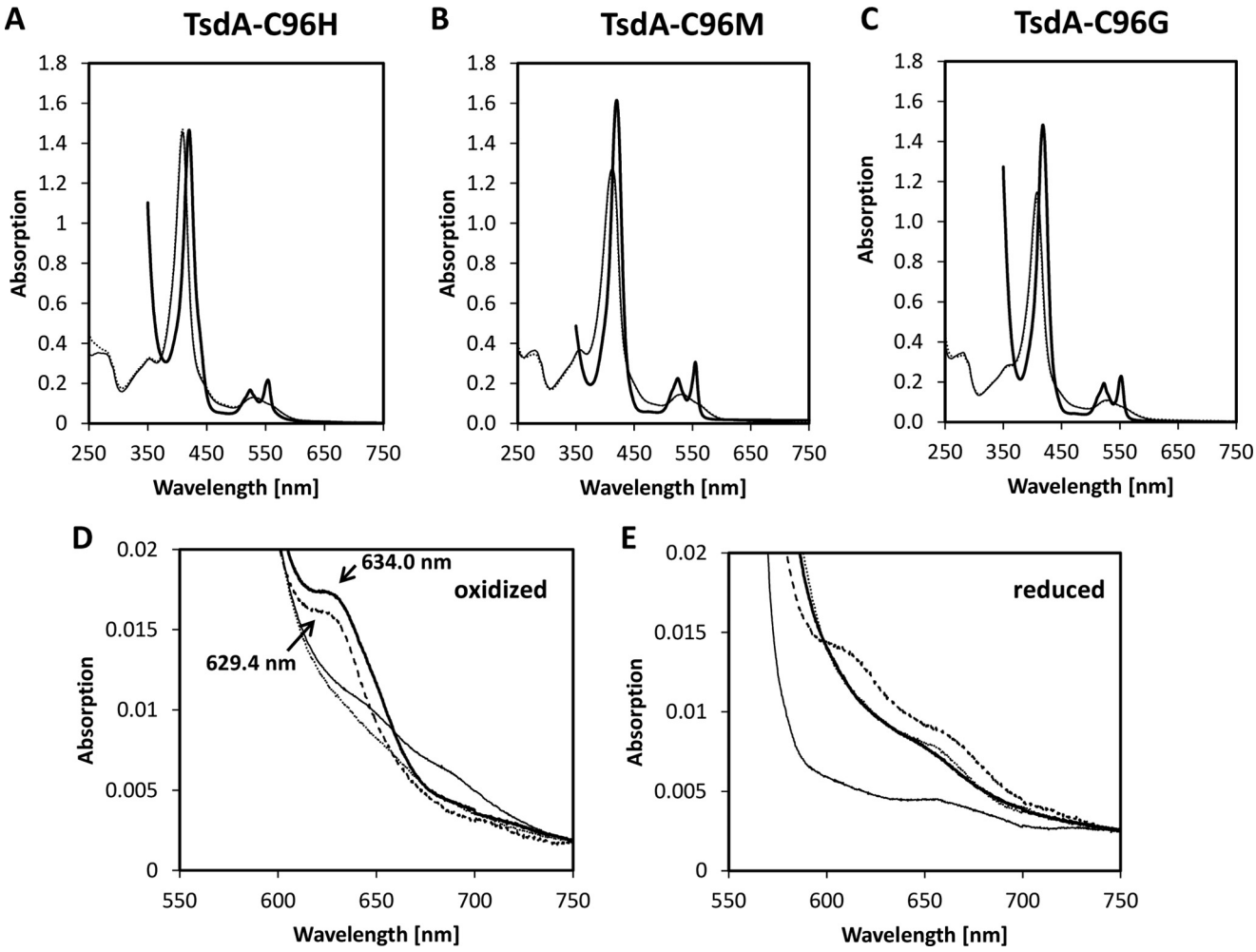

FIGURE 6. **Comparison of electronic absorbance spectra for *A. vinosum* TsdA Cys^{96} variants.** Complete spectra of recombinant TsdA-C96H (100 μg ml^{-1}; 3.6 μM) (*A*), TsdA-C96M (120 μg ml^{-1}; 4.3 μM) (*B*), and TsdA-C96G (125 μg ml^{-1}; 4.5 μM) (*C*) were recorded for the "as isolated" (*thin line*), oxidized (*dotted line*), and reduced states (*thick line*). The region from 550 to 750 nm is *enlarged* for the oxidized (*D*) and reduced (*E*) state of recombinant TsdAwt (250 μg ml^{-1}; 8.9 μM; *thick line*), TsdA-C96G (*dashed line*), TsdA-C96H (*dotted line*), and TsdA-C96M (*thin line*). Oxidation was achieved by the addition of 3.5 μM ferricyanide, and reduction was achieved by the addition of 10 mM sodium dithionite. All spectra were recorded in 50 mM BisTris-HCl buffer, pH 6.5, and set to the same 280 and 750 nm values.

K208G variant II, Cys^{96} is persulfurated with a partially occupied sulfite in its vicinity and a thiosulfate further away, close to the cleft's entrance (Fig. 5*C*, PDB 4WQE). One oxygen of this thiosulfate is only 2.7 Å away from the water molecule that is close to the sulfite and at the same spatial position as the S1 atom of thiosulfate present in the two structures depicted in Fig. 4, *A* and *C* (PDB entries 4QWC and 4QW9). Based on these structures with various ligands, a tetrathionate was manually fitted into the TsdA active site (Fig. 5*D*).

Site-directed mutagenesis studies of Cys^{96}—The structural data proved our hypothesis that Cys^{96} acts as the sixth distal ligand of heme 1. We have previously reported studies with a TsdA-C96G variant in which the heme ligating cysteine was exchanged by glycine, an amino acid not capable of heme coordination (1). Now, we also replaced Cys^{96} with histidine and methionine, which should be capable of heme iron coordination. TsdA-C96H and TsdA-C96M were produced successfully and analyzed by gel filtration. All three TsdA cysteine mutant proteins behaved as monomers and showed the expected size of 28 kDa upon SDS-PAGE (not shown). Electronic absorption spectra strongly indicated that methionine and histidine acted as ligands to heme 1 in the respective variant proteins. First, the Soret peak shifted to a longer wavelength and increased in intensity (Fig. 6 and Table 4), consistent with replacement of Cys^{96} with a stronger field ligand in both cases (52). Second, spectral features characteristic for five-coordinate high-spin heme (52) were not present. An absorbance band at 695 nm, usually indicating methionine ligation, was not observed for the TsdA-C96M variant (Fig. 6*B*) (53). It should be noted, however, that some methionine-ligated hemes do not exhibit a peak at this wavelength (54). As opposed to the other two variants, TsdA-C96G exhibited a low-intensity spectral feature indicative of the presence of pentacoordinated high-spin heme (Fig. 6*D*) (*i.e.* a band at 630 nm in the oxidized state) (53).

Activity in the thiosulfate-oxidizing as well as in the tetrathionate-reducing direction was completely abolished in all of the TsdA Cys^{96} variants (Table 5). In addition, it was not possible to reduce any of the TsdA cysteine variants with thiosulfate (not shown). All of these findings clearly indicate Cys^{96} as an essential active site residue.

TABLE 4
Spectral characteristics of TsdA wild-type protein and TsdA variants in the oxidized and reduced state

Protein (pH)	Soret oxidized	δ-Peak	Soret reduced	α-Peak	β-Peak	$E_{Soret(ox)}/E_{280\ nm}$	$E_{Soret(red)}/E_{\alpha}$	E_{α}/E_{β}	Charge transfer
	nm	*nm*	*nm*	*nm*	*nm*				*nm*
TsdAwt (pH 5.0)	406	354	417	552	523	3.2	6.8	1.3	No
TsdAwt (pH 6.5)	407	357	420	555	524	3.3	5.9	1.3	634 (ox)
TsdAwt (pH8.0)	407	357	420	554	524	3.2	5.0	1.3	636 (ox)
TsdA-C96G (pH 6.5)	407	353	419	554	523	4.1	6.8	1.2	629 (ox)
TsdA-C96H (pH 6.5)	409	353	420	554	524	4.1	6.8	1.3	660 (red)
TsdA-C96 M (pH 6.5)	411	360	420	555	525	4.3	5.3	1.4	660 (red)
TsdA-K208N (pH 6.5)	413	358	420	555	524	2.7	5.4	1.3	620; 695 (ox)
TsdA-K208G (pH 6.5)	406	357	420	555	524	2.8	4.7	1.4	621; 697 (ox)
TsdA-M209G (pH 6.5)	405	351	417	553	523	3.1	5.1	1.7	630 (ox)

TABLE 5
Kinetic characteristics of thiosulfate oxidation and tetrathionate reduction catalyzed by TsdA wild type protein or TsdA variants

	Thiosulfate → ferricyanide (pH 4.0)				Thiosulfate → ferricyanide (pH 5.0)				Methylviologen → tetrathionate (pH 5.0)			
	V_{max}	k_{cat}	$S_{0.5}$	$k_{cat}/S_{0.5}$	V_{max}	k_{cat}	$S_{0.5}$	$k_{cat}/S_{0.5}$	V_{max}	k_{cat}	$S_{0.5}$	$k_{cat}/S_{0.5}$
	units mg−1	s^{-1}	*mM*	$mM^{-1}\ s^{-1}$	*units* mg^{-1}	s^{-1}	*mM*	$mM^{-1}\ s^{-1}$	*units* mg^{-1}	s^{-1}	*mM*	$mM^{-1}\ s^{-1}$
TsdA	28,600 ± 2500	14,000	1.1 ± 0.2	13,000	4470 ± 430	2010	0.14 ± 0.06	14,100	82.0 ± 3.4	37	1.98 ± 0.32	18.7
TsdA-K208G	2370 ± 410	1070	1.1 ± 0.5	970	810 ± 90	370	0.46 ± 0.17	790	93.9 ± 10.0	42	1.17 ± 0.40	35.9
TsdA-K208N	1470 ± 170	660	1.3 ± 0.3	510	780 ± 80	350	0.17 ± 0.06	2100	80.0 ± 17.0	36	3.20 ± 1.40	11.3
TsdA-M209G	2900 ± 130	1330	0.9 ± 0.1	1480	1700 ± 130	760	1.08 ± 0.22	710	121 ± 11.5	54	1.16 ± 0.13	46.7
TsdA-C96M/H/G												

Heme 2 Undergoes a Ligand Switch upon Reduction—Similarly to heme 1, heme 2 is also quite solvent-exposed, although only one of its propionate groups (bound to the pyrrole ring D), is oriented toward the solvent with Arg^{50} and His^{51} in its vicinity (Fig. 3*D*). Toward the interior of the protein, the second propionate arm and pyrrole ring B stack against a wall of hydrophobic residues, such as Pro^{4}, Leu^{179}, Phe^{180}, and Leu^{211}. Interestingly, Leu^{179} and Phe^{180} shape a protuberance over the heme, making this entrance somewhat narrower than in heme 1. Lys^{208}, the distal axial ligand to heme 2 in oxidized TsdA, and the neighboring Met^{209} are located close to the surface of the protein followed by a flexible loop (Pro^{210}–Leu^{216}) that is disordered in all data sets analyzed.

Most remarkably, when crystals of *A. vinosum* TsdA are reduced by soaking with bisulfite or dithionite, Lys^{208} is replaced by the adjacent Met^{209} as the distal axial ligand (Fig. 4*D*). When Met^{209} coordinates heme 2, Lys^{208} switches its position, with the side chain now pointing toward a turn between two helices, helix II_N and another helix not part of the classical class II *c*-type cytochrome. The side chain of Lys^{208} is now within hydrogen bonding distance to the carboxylate of Glu^{63} and main chain carbonyl oxygen of Ala^{64}. In some other TsdA structures, the side chain of Glu^{63} shows a different rotamer or an alternate conformation, suggesting flexibility around this residue. Interestingly, no major backbone conformational changes are observed upon ligand switch; only the end of helix II_C, where Lys^{208} and Met^{209} sit, unwinds along with a positional adjustment of the following residues (Figs. 2*B* and 4*C*). The loop comprising residues Leu^{211}–Leu^{216} is not ordered.

Site-directed Mutagenesis of Lys^{208}—TsdA variants were constructed in which the unusual lysine ligand of heme 2 was replaced not only by glycine (TsdA-K208G) but also by asparagine (TsdA-K208N), thereby creating the situation observed in the vast majority of TsdAs from other organisms. An asparagine residue at the Lys^{208} equivalent position is highly conserved among proteobacterial thiosulfate dehydrogenases and, for example, found in TsdA from the β-proteobacteria *Cupriavidus metallidurans*, *Thiomonas intermedia*, and *Sideroxydans lithotrophus* as well as in the pathogenic ε-proteobacterium *Campylobacter jejuni* (1). Even *Marichromatium purpuratum*, a member of the same γ-proteobacterial family as *A. vinosum*, possesses a TsdA homologue (AHF02870.1) with an Asn residue instead of Lys^{208}. The ε-proteobacterium *Wolinella succinogenes* is a notable exception and contains a TsdA homologue (NP_906283.1) with a Thr residue instead of the highly conserved asparagine.

Both *A. vinosum* TsdA Lys^{208} variants behaved as monomers upon analytical gel filtration and exhibited the expected size of 28 kDa in SDS-PAGE (not shown). Similar values for $Soret_{red}$/280 nm for TsdA Lys mutants and TsdA wild type protein proved full heme loading (Table 5). Both TsdA Lys^{208} variants were catalytically active in thiosulfate oxidation as well as in tetrathionate reduction (Table 5), thus supporting heme 1 as the active site and suggesting heme 2 as the electron exit point.

In the crystal structures of the TsdA-K208N and TsdA-K208G variants, His^{164} and Met^{209} are coordinating heme 2 (Fig. 5, *A* and *B*); the environment around the heme 2 distal ligand is highly disordered and, although modeled, displays high thermal motion parameters (*B* factors) and some unexplained electron density, which we attribute to different conformations of the loop. It is plausible to assume that the introduction of an amino acid residue without any side chain conferred on the terminal portion of helix II_C an extra degree of freedom (note that the disordered loop in the "as isolated" structure starts at Pro^{210}), making this loop extremely flexible and difficult to model. Nevertheless, there is no doubt that Met^{209} is the distal ligand in this TsdA variant. This is corroborated by electronic absorption spectroscopy, which indicated Met^{209} as the sixth ligand to heme 2 when Lys^{208} is replaced by either glycine or asparagine (Fig. 7 and Table 4). This was evident by the new charge transfer band around 695 nm indicative of Met-coordinated heme iron (53) in the oxidized variant pro-

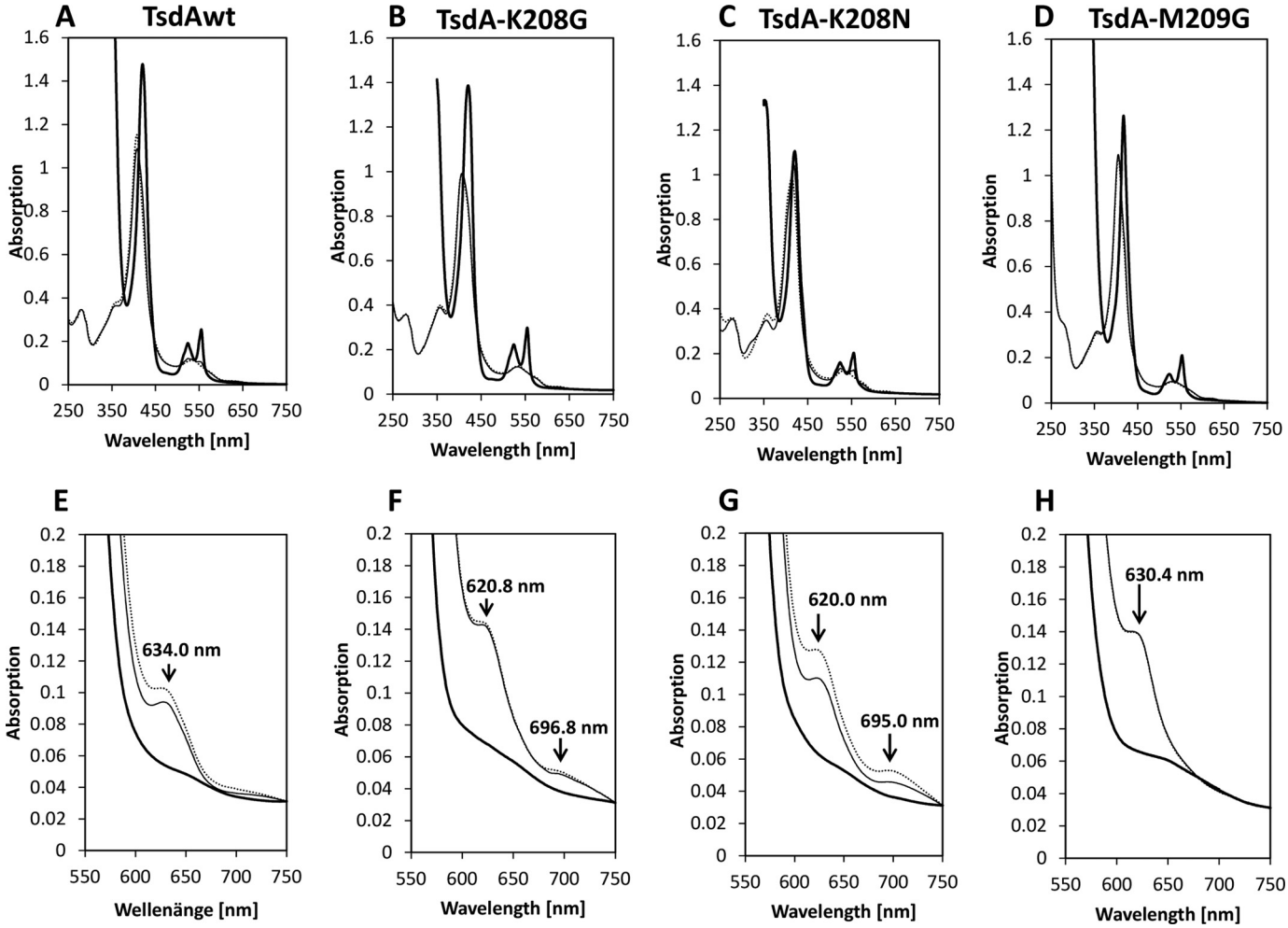

FIGURE 7. **Comparison of electronic absorbance spectra for *A. vinosum* TsdA wild type and Lys^{208}/Met^{209} variants.** Complete spectra of recombinant TsdA wild type (160 μg ml^{-1}; 5.7 μM) (*A*), TsdA-K208G (224.6 μg ml^{-1}; 8.3 μM) (*B*), TsdA-K208N (200 μg ml^{-1}; 7.4 μM) (*C*), and TsdA-M209G (218 μg ml^{-1}; 8.1 μM) (*D*) were recorded for the "as isolated" (*thin line*), oxidized (*dotted line*), and reduced states (*thick line*). Oxidation was achieved by the addition of 7 μM ferricyanide, and reduction was achieved by the addition of 10 mM sodium dithionite. Spectra from 550 to 750 nm were recorded for highly concentrated protein solutions: TsdA wild type protein (1150 μg ml^{-1}; 41.1 μM) (*E*), TsdA-K208G (100 μg ml^{-1}; 37 μM) (*F*), TsdA-K208N (1123 μg ml^{-1}; 41.6 μM) (*G*), and TsdA-M209G (873 μg ml^{-1}; 32.3 μM) (*H*). All spectra were taken in 50 mM BisTris-HCl buffer, pH 6.5, and set to the same 280 and 750 nm values.

teins (Fig. 7, *F* and *G*). The finding that Met^{209} serves as the ligand for the heme 2 iron in oxidized TsdA-K208N shows that the weak field ligand asparagine cannot functionally replace lysine.

In a last experiment, we replaced Met^{209} by glycine. Electronic absorption spectroscopy indicated the presence of five-coordinate high-spin heme in this variant due to the presence of a band at 630 nm (Fig. 7*H*) (53). Activity was still present in both the thiosulfate-oxidizing and tetrathionate-reducing directions (Table 5). A conspicuous difference was observed with regard to $S_{0.5}$ for thiosulfate. This value rose by a factor of 5 at pH 5.0 (Table 5). A similar effect was caused by the Lys^{208} → Gly replacement (Table 5). Both observations hint at a possible cooperativity between the two hemes that needs to be further elucidated in the future.

pH Dependence of Activity and Electronic Absorption Spectra—Redox transformations of cysteine-bound hemes are often accompanied by protonation or deprotonation reactions of the essential cysteine ligand. Such reactions cannot be assessed by structural analysis alone, and we therefore performed an independent set of experiments analyzing the effect of pH on TsdA activity and electronic absorption spectra.

Consistent with earlier results (1), V_{max} for thiosulfate-dependent reduction of the artificial electron acceptor ferricyanide proved to be about 5 times lower at pH 5.0 than at pH 4.0 (4470 *versus* 28,600 units/mg; Table 5), whereas $S_{0.5}$ for thiosulfate decreased from 1.1 mM at pH 4.0 to 0.14 mM at pH 5.0 This results in a 15% higher value for $k_{cat}/S_{0.5}$ at pH 5.0 than at pH 4.0 (Table 5), implying that TsdA is even slightly more efficient in converting thiosulfate to tetrathionate at pH 5.0. At pH 5.0, we also analyzed the tetrathionate reduction ability with reduced methylviologen as artificial electron donor of the TsdA wild type protein. The enzyme exhibited very low specific activity (V_{max} of 82 units/mg) and a relatively high $S_{0.5}$ of 1.98 mM for tetrathionate, resulting a k_{cat} of 37 s^{-1} and $k_{cat}/S_{0.5}$ = 18.7 (Table 5). These findings agree with earlier work that identified *A. vinosum* TsdA wild type as a more efficient thiosulfate dehydrogenase than tetrathionate reductase (2).

In a second approach, we used electronic absorption spectroscopy to collect experimental evidence for protonation/de-

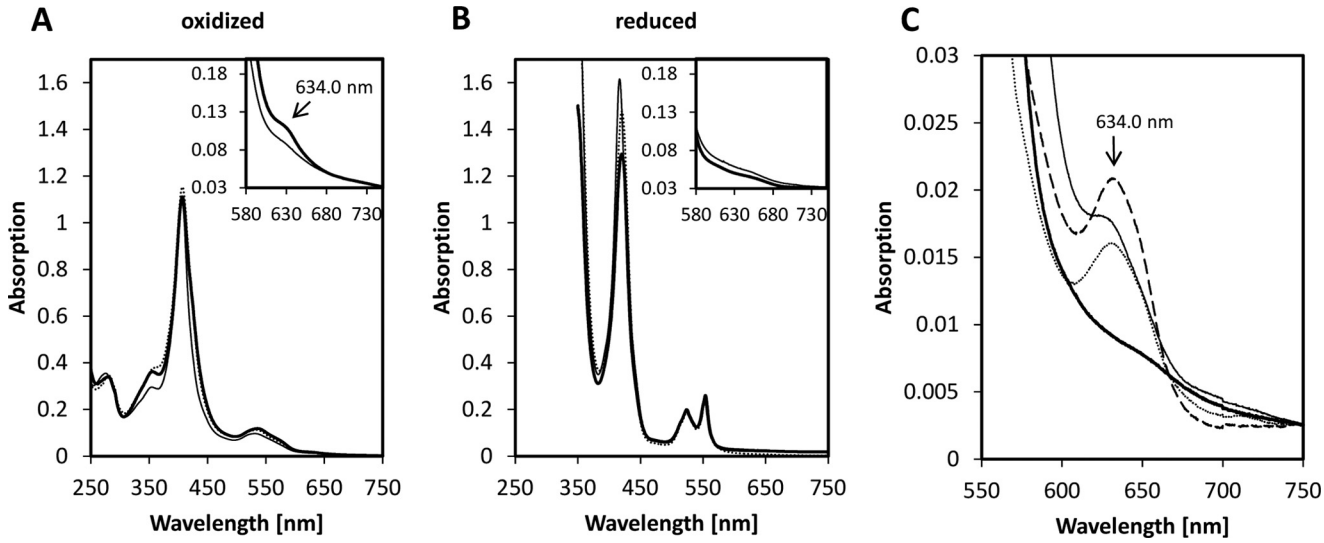

FIGURE 8. **Comparison of electronic absorption spectra for the *A. vinosum* TsdA wild type protein at different pH values.** Spectra of recombinant TsdA wild type protein (160 μg ml^{-1}; 5.9 μM) at pH 5.0 (*thin line*), pH 6.5 (*dotted line*), and pH 8 (*thick line*) in the oxidized (*A*) and in the reduced state (*B*) were recorded in 100 mM ammonium acetate buffer (pH 5.0), 50 mM BisTris-HCl buffer (pH 6.5), or 50 mM Tris-HCl buffer (pH 8.0), respectively. Oxidation was achieved by the addition of 7 μM ferricyanide, and reduction was achieved by the addition of 10 mM sodium dithionite. The *insets* in *A* and *B* show details of the 580–750 nm region (640 μg ml^{-1}; 23.7 μM). *C*, comparison of electronic absorption spectra (550–750 nm) for *A. vinosum* wild type TsdA (160 μg ml^{-1}; 5.9 μM) in the oxidized (*thin line*), thiosulfate-reduced (*dotted line*), partially reduced (*dashed line*), and completely reduced (*thick line*) state. Partial reduction was achieved by the addition of 1 mM sodium dithionite, and complete reduction was achieved by the addition of 10 mM sodium dithionite. For the thiosulfate-reduced state, 2 mM thiosulfate were added. All spectra were recorded in 50 mM BisTris-HCl buffer, pH 6.5.

protonation reactions of the active site cysteine in TsdA. This is possible because changes in the protonation state of thiol (thiolate)-bound hemes are often associated with large shifts in the Soret spectral region (54). Indeed, for the reduced *A. vinosum* enzyme, an increase in pH significantly altered the electronic spectrum (Fig. 8). The Soret band maximum of the reduced protein was red-shifted (from 417 to 420 nm), whereas the intensity of the band significantly decreased with increasing pH (Fig. 8*B*). This is indicative for the presence of a stronger field ligand of the heme iron at higher pH (52). At a lower pH, the cysteine thiolate is probably protonated, and the Cys^{96} thiol would be a weaker ligand to the heme (54). For the oxidized protein, the Soret band maximum remained at 406 nm even at pH 8.0 (Fig. 8*A*), indicating retention of thiolate ligation.

In the oxidized state of the TsdA wild type protein, a peak at 634 nm was observed at pH 6.5 and pH 8.0 but not at pH 5.0 (Fig. 8*A*, *inset*). In the completely reduced state of the protein, the band was not present (Figs. 6*D* and 8*B*, *inset*). A band at the same position has been reported to be indicative for thiolate-ligated heme (55). This interpretation is corroborated by the fact that the 634 nm absorbance band is absent in all TsdA variants with replacements of Cys^{96} (Fig. 6*D* and Table 3) but present (albeit at about 620 instead of 634 nm) in the TsdA Lys^{208} mutant proteins (Fig. 7, *F* and *G*, and Table 4).

The 634 nm band became more pronounced when wild type TsdA was partially reduced with its natural substrate thiosulfate or by the addition of 1 mM sodium dithionite (Fig. 8*C*), pointing at the transient presence of high-spin heme (53), possibly caused by movement of Cys^{96} out of the iron coordination sphere. This conclusion is supported by the presence of a structural conformer in which Cys^{96} is tilted away from the heme-coordinating position, as described above.

In contrast, the 634 nm intermediate state band observed for the TsdA wild type protein was completely absent in the Cys^{96} mutant proteins, unambiguously allocating this spectral feature to heme 1 (Fig. 6 and Table 4).

DISCUSSION

In this work, we performed a thorough structural and biochemical analysis of a purple bacterial thiosulfate dehydrogenase. The protein was found to contain two heme groups, both with unusual axial coordination. In the oxidized state, heme 1 has a His^{53}/Cys^{96} ligation, whereas heme 2 is coordinated by His^{164}/Lys^{208}. All tested TsdA Cys^{96} variants were catalytically inactive both in the thiosulfate-oxidizing as in the tetrathionate-reducing direction. In contrast, all TsdA Lys^{208} variants retained activity. This identifies Cys^{96} as an active site residue and emphasizes a general important role for cysteine in proteins containing His/Cys-ligated hemes (6, 8, 22, 23). One other example where replacement of the heme-ligating cysteine inactivated the protein *in vivo* is the *A. vinosum* triheme cytochrome DsrJ (22). Most data are available for the heterodimeric SoxXA protein. Its SoxA subunit is a diheme protein in *R. sulfidophilum* and *Paracoccus pantotrophus* (8), whereas only the heme corresponding to TsdA heme 1 is present in SoxA from *Starkeya novella*. In all cases, the His/Cys-ligated heme equivalent to TsdA heme 1 has been shown to participate in the SoxXA-catalyzed reaction (7, 20, 50, 56). However, it is still a matter of debate to what extent the heme-ligating cysteine is involved in the reaction and how it exerts its function. The His/Cys ligation corresponds to an extremely low redox potential of the corresponding heme in SoxA and DsrJ (23, 57–59). Values of -432 ± 15 and -479 ± 10 mV (*versus* NHE at pH 7.0) have been reported for the SoxA hemes in *P. pantotropus* and *S. novella* SoxA (12, 14). Thus, considering the E_m of +24 mV for the thiosulfate/tetrathionate couple (60), the Cys coordination of heme 1 as the electron entry point appears somewhat

surprising because it would imply a highly unlikely electron transfer from thiosulfate oxidation to TsdA heme 1.

A positively charged cavity found next to heme 1 and Cys^{96} probably constitutes the active site of TsdA. In two structures, we observed a bound thiosulfate in the proposed active site region. This region appears to be rather similar to that described for SoxA (6, 7, 50, 61), where in both cases, several arginine residues are expected to create a strong positive electrostatic field suited for binding the anionic substrate thiosulfate. Bamford *et al.* (21) suggested that the active site cysteine in SoxA is stabilized in its thiolate form (or the persulfide thereof) by its coordination to the ferric *c*-type heme. Indeed, a thiolate can be expected to be preferred over a thiol as a ligand for an oxidized heme, where the metalloporphyrin dianion unit has a core charge of +1 (54). Furthermore, it was proposed that the basic residues in the vicinity of the active site contribute to stabilization of the cysteinate form (6). For *R. sulfidophilum* SoxXA, it has been discussed that the thiolate ligand temporarily dissociates from the heme and covalently binds the thiosulfate substrate, resulting in a SoxA-thiocysteine *S*-sulfate intermediate state, accompanied by reduction of the catalytic heme and a second heme present in the SoxX subunit (6). In this mechanism, the oxidized thiosulfate would subsequently be transferred to a cysteine residue present in the SoxY subunit of the SoxYZ carrier protein. Catalysis by SoxA would thus essentially follow a rhodanese-like mechanism involving a thiosulfate transfer reaction. On the other hand, an *S. novella* SoxXA variant with a Cys-Met exchange was still catalytically competent *in vitro*, and it was concluded that the cysteine is not absolutely crucial for SoxXA activity, making a purely rhodanese-like SoxXA reaction mechanism unlikely (7).

The crystallographic data acquired in our study are in principle consistent with different catalytic mechanisms. The thiosulfate molecule observed in two of the structures (Fig. 4, *A* and *C*) closely approaches both Cys^{96} and the heme 1 iron, and the possibility of a sulfur transferase-like mechanism similar to what has been suggested for SoxXA cannot be discounted (6). However, different interpretations are possible for the results reported herein. The importance of Cys as an active site ligand may lie in its ability to act as a switch. It could keep the heme in a low-redox potential oxidized state but would be a weak enough ligand that it could be moved out of the coordination sphere when thiosulfate enters the active site, thus leading to a strong increase in the heme's redox potential. This suggestion corresponds to the alternative Cys^{96} conformation observed in some structures. Combination of two thiosulfate molecules at the active site, liberating two electrons, could then proceed with reduction of the two hemes of TsdA. This suggestion conforms in part to an alternative reaction mechanism discussed recently for SoxXA (57). Whereas Bradley *et al.* (57) promoted the idea that SoxXA might mediate the direct coupling of thiosulfate to SoxY without dissociation of any heme ligands, we consider the possibility that Cys^{96} temporarily exits the heme 1 iron coordination during the reaction cycle, leading to a change in the redox potential such that electron transfer into heme 1 is facilitated. The observed switch at heme 2 from His/Lys to His/Met ligation upon reduction, leading to greater disparity in redox potential between heme 1 and heme 2 (discussed in more detail below), could be a further means to drive the reaction to tetrathionate production. We showed in this work that the Sγ of Cys^{96} can adopt a second conformation tilted away from the heme 1 iron and out of its coordination sphere. TsdA exhibits higher specific activity at low pH, which is consistent with the idea that in its protonated form, the Sγ of Cys^{96} is a weaker ligand to heme iron that should be more prone to move into the non-iron-coordinating alternate position, promoting catalysis. Furthermore, we showed that when we replaced Cys^{96} by the stronger field ligands methionine and histidine, the activity of the enzyme was completely abolished. For the *R. sulfidophilus* SoxXA, it has also been proposed that the thiolate ligand to the active site heme is protonated upon reduction (20, 57). It is difficult to envision how a protonated cysteine could be a suitable acceptor for covalent attachment of thiosulfate.

The structural flexibility of Cys as heme ligands has been reported for the several proteins where they are present, including SoxA (7, 8, 23). It is a matter of discussion whether this flexibility is a prerequisite for catalysis (59). In the case of TsdA, the flexibility of the active site Cys observed by EPR spectroscopy (1), and especially the movement of Sγ of Cys^{96} out of the heme coordination sphere documented in this work by structural and spectroscopic evidence, is highly likely to enable the transient formation of high-spin iron. Our finding that the TsdA-C96G variant has no residual activity contradicts a reaction mechanism that mainly relies on the transient formation of a pentacoordinated state of the catalytic heme, because glycine should *per se* not be able to act as a heme ligand. On the other hand, this protein variant presents only a low-intensity high-spin signal in the electronic absorbance spectra, indicating that a major heme population may have coordination by water or another exogenous ligand, resulting in a protein state that is not catalytically competent. Further experiments are necessary to clarify this question.

Previously, a critical role for a post-translational cysteine persulfide modification of the SoxA heme ligand for SoxXA has been suggested (6). Whereas in the two structures of SoxXA from *R. sulfidophilum* and *P. pantotrophus*, the cysteines at the active site hemes were found to be quantitatively modified to cysteine persulfide, in the *S. novella* structure, the coordinating residue was modeled as an equal mixture of Cys and cysteine persulfide (7). The detection of the persulfide has been taken as an indication that sulfur substrates, such as thiosulfate, could indeed become temporarily bound to the heme-ligating residue, and it has been proposed that incomplete catalysis (*i.e.* transfer of solely the thiosulfate sulfone sulfur instead of the complete thiosulfate moiety to SoxYZ) is the cause for persulfuration of the active site cysteine (6). It should however, be noted that even recombinant SoxA that had been produced in *E. coli* in the absence of thiosulfate or other Sox pathway proteins carried the modification, at least in part of the protein molecules (7, 57). The *A. vinosum* TsdA and all its variants studied here were recombinantly expressed in *E. coli*, and we also observed partial persulfide modification in some structures. It is noteworthy that in some of these structures, we observe a sulfite molecule at the active site, which we interpret as the product of reaction with thiosulfate, possibly present in the growth medium, leading to formation of the Cys persulfide

and sulfite. The possibility exists that the modification is not crucial for catalysis and that it arises from a side reaction, at least in TsdA. The Cys^{96} thiolate may be prone to modification when a suitable electron acceptor is not present.

In the structure derived from a dithionite-reduced crystal, thiosulfate was evident in the active site pocket with the sulfane group oriented toward the heme plane (Fig. 4*C*). Furthermore, in some other structures, the same position is occupied by a sulfite and a water molecule. Taken together, their arrangement closely resembles the spatial organization of thiosulfate with the S1–S2 bond (or the S1 atom of sulfite and the oxygen atom of water) oriented such that the sulfane group is pointing toward the heme plane (Fig. 5*C*). In none of the structures did we observe a covalent adduct between the thiosulfate molecule and Cys^{96}.

Although the back-reaction has never been discussed for the SoxXA-catalyzed reaction, and it is indeed irrelevant *in vivo* in this case, it is proven that TsdAs can be even more adapted for catalysis of tetrathionate reduction, as in, for example, the enzyme from *C. jejuni* (2). Although it is not clear in detail which modifications lead to the observed changes in catalytic efficiencies, it is clear from sequence comparisons that this does not involve major changes in the active site residues (1, 2). A mechanism including formation of a covalent thiocysteine *S*-sulfate intermediate from tetrathionate would involve two serial cleavages of sulfur-sulfur bonds, the first occurring between the two central atoms of tetrathionate and the second occurring between Sγ of Cys^{96} and the thiosulfate moiety. Our structural data neither directly exclude nor support such a mechanism, although it is difficult to envision a molecule with the size of tetrathionate approaching Cys^{96} close enough for direct reaction with the thiolate.

In one of the structures for the TsdA-K208G variant (PDB 4WQE), a thiosulfate molecule mimicked by sulfite and a water molecule is oriented close to Cys^{96} with the help of Arg^{82} and Arg^{92}, and a second thiosulfate is present in close vicinity (Fig. 5*C*). It is striking that a tetrathionate molecule modeled into this structure superimposes almost exactly on the thiosulfate plus water and sulfite molecules (Fig. 5*D*). Thus, this structure reveals how two thiosulfate molecules could fit in the active site before the covalent bond is formed between their sulfane sulfur atoms.

It is clear from the structural analyses presented here that TsdA heme 2 is ligated by Lys^{208} in the oxidized state of the enzyme. Oxidation of two thiosulfate molecules to tetrathionate releases two electrons that can be accommodated by the two heme groups of TsdA. We showed that a switch occurs at heme 2 from Lys to Met axial ligation upon reduction. Many six-coordinate heme proteins are known to swap ligands upon reduction/oxidation, and such changes affect the redox potential of the hemes (15, 62). Ligand motifs that favor binding to Fe(III) heme generally result in more negative reduction potential values than ligand motifs that favor binding to Fe(II). Soft ligands, such as methionine, stabilize reduced iron, which results in a positive shift in E_m values (15, 62). On the basis of these considerations, heme 2 is predicted to be more positive in potential in the His/Met than in the His/Lys-ligated state. This should lead to marked hysteresis in electrochemical measurements (63) and can be experimentally verified in the future. The

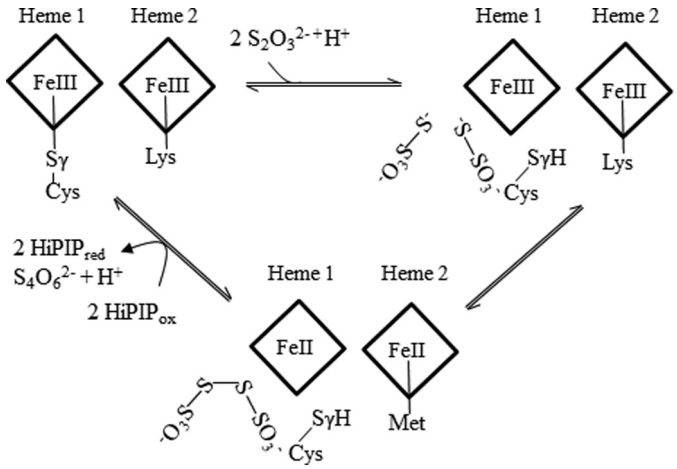

FIGURE 9. **Proposed mechanism of TsdA activity.** A reaction scheme for the TsdA-catalyzed oxidation of two thiosulfate molecules to tetrathionate is shown. Two thiosulfate molecules enter the active site, inducing the Sγ atom of Cys^{96} to tilt away from the iron coordination sphere. This is probably accompanied by protonation of Sγ. The two thiosulfates react directly with each other, liberating two electrons that reduce heme 1 and heme 2. Upon reduction, heme 2 undergoes a shift from His/Lys to His/Met ligation. Tetrathionate is released, and the hemes are oxidized. HiPIP (high-potential iron-sulfur protein) is a likely *in vivo* electron acceptor for *A. vinosum* TsdA (64). Cys^{96} is deprotonated, and Sγ is re-established as the ligand to heme 1 iron.

ligand change could thus guide the catalytic electron transfer event such that the gate for the back-reaction is closed upon reduction of heme 2, because the positive redox potential of the His/Met ligated heme hinders its reoxidation.

Overall, our kinetic, spectroscopic, and structural data lead us to propose the following mechanism for thiosulfate oxidation (Fig. 9). Two thiosulfate molecules enter the active site, which probably induces a movement of the Sγ of Cys^{96} out of the iron coordination sphere. This ligand movement results in an increase of the redox potential of heme 1, thus allowing the sequential uptake of the two electrons resulting from the conversion of the two thiosulfates to tetrathionate, leading to the reduction of both hemes. Upon reduction, heme 2 undergoes a ligand switch, which increases its redox potential and hinders the back-reaction. The high-potential iron-sulfur protein (HiPIP) is a likely electron acceptor for the *A. vinosum* TsdA *in vivo* (64).

CONCLUSIONS

In summary, we provide a thorough functional and structural characterization of *A. vinosum* TsdA and propose a catalytic mechanism for this enzyme. We established the His/Cys-ligated heme 1 and the His/Lys-ligated heme 2 as the catalytic and electron transfer hemes, respectively. The heme 1-ligating Cys^{96} was shown to be essential for catalysis, and heme 2 was shown to undergo a ligand switch with Met^{209} replacing Lys^{208} as an axial ligand to heme 2 in the reduced state. Future experiments, including magnetic circular dichroism spectroscopy or synchrotron-based x-ray-induced photoreduction experiments coupled with single crystal microspectrophotometry may shed light on short lived intermediates and redox states of the enzyme and may help to clarify the reaction mechanism.

Acknowledgments—We thank colleagues at the Macromolecular Crystallography Unit at ITQB-UNL (Oeiras, Portugal) for collecting diffraction data and the beamline scientists at the ALBA, PETRA III, ESRF, SLS, and Diamond synchrotrons for technical support during data collection. Experiments were performed on the XALOC beamline at ALBA synchrotron (Barcelona, Spain), the P14 beamline at PETRA III synchrotron (Hamburg, Germany), the X06DA beamline at Swiss Light Source (SLS, Villigen, Switzerland), the I02 beamline at Diamond Light Source (DLS, Didcot, UK), and the ID29 beamline at the European Synchrotron Radiation Facility (ESRF, Grenoble, France). We are grateful to the Local Contacts and Beamline Scientists in all these beamlines for providing assistance and technical support during diffraction data experiments, and to the colleagues from the Macromolecular Crystallography Unit at ITQB-UNL for collecting diffraction data.

REFERENCES

1. Denkmann, K., Grein, F., Zigann, R., Siemen, A., Bergmann, J., van Helmont, S., Nicolai, A., Pereira, I. A. C., and Dahl, C. (2012) Thiosulfate dehydrogenase: a wide-spread unusual acidophilic *c*-type cytochrome. *Environ. Microbiol.* **14,** 2673–2688
2. Liu, Y.-W., Denkmann, K., Kosciow, K., Dahl, C., and Kelly, D. J. (2013) Tetrathionate stimulated growth of *Campylobacter jejuni* identifies TsdA as a new type of bi-functional tetrathionate reductase that is widely distributed in bacteria. *Mol. Microbiol.* **88,** 173–188
3. Imhoff, J. F., Süling, J., and Petri, R. (1998) Phylogenetic relationships among the *Chromatiaceae*, their taxonomic reclassification and description of the new genera *Allochromatium*, *Halochromatium*, *Isochromatium*, *Marichromatium*, *Thiococcus*, *Thiohalocapsa*, and *Thermochromatium*. *Int. J. Syst. Bacteriol.* **48,** 1129–1143
4. Hensen, D., Sperling, D., Trüper, H. G., Brune, D. C., and Dahl, C. (2006) Thiosulphate oxidation in the phototrophic sulphur bacterium *Allochromatium vinosum*. *Mol. Microbiol.* **62,** 794–810
5. Friedrich, C. G., Bardischewsky, F., Rother, D., Quentmeier, A., and Fischer, J. (2005) Prokaryotic sulfur oxidation. *Curr. Opin. Microbiol.* **8,** 253–259
6. Bamford, V. A., Bruno, S., Rasmussen, T., Appia-Ayme, C., Cheesman, M. R., Berks, B. C., and Hemmings, A. M. (2002) Structural basis for the oxidation of thiosulfate by a sulfur cycle enzyme. *EMBO J.* **21,** 5599–5610
7. Kilmartin, J. R., Maher, M. J., Krusong, K., Noble, C. J., Hanson, G. R., Bernhardt, P. V., Riley, M. J., and Kappler, U. (2011) Insights into structure and function of the active site of SoxAX cytochromes. *J. Biol. Chem.* **286,** 24872–24881
8. Kappler, U., and Maher, M. J. (2013) The bacterial SoxAX cytochromes. *Cell Mol. Life Sci.* **70,** 977–992
9. Lemberg, R., and Barrett, J. (1973) *Cytochromes*, Academic Press, Inc., New York
10. Wood, P. M. (1983) Why do *c*-type cytochromes exist? *FEBS Lett.* **164,** 223–226
11. Simon, J. (2002) Enzymology and bioenergetics of respiratory nitrite ammonification. *FEMS Microbiol. Rev.* **26,** 285–309
12. Hartshorne, R. S., Kern, M., Meyer, B., Clarke, T. A., Karas, M., Richardson, D. J., and Simon, J. (2007) A dedicated haem lyase is required for the maturation of a novel bacterial cytochrome *c* with unconventional covalent haem binding. *Mol. Microbiol.* **64,** 1049–1060
13. Einsle, O., Stach, P., Messerschmidt, A., Simon, J., Kröger, A., Huber, R., and Kroneck, P. M. (2000) Cytochrome *c* nitrite reductase from *Wolinella succinogenes*: structure at 1.6 Å resolution, inhibitor binding, and heme-packing motifs. *J. Biol. Chem.* **275,** 39608–39616
14. Einsle, O., Stach, P., Messerschmidt, A., Klimmek, O., Simon, J., Kröger, A., and Kroneck, P. M. (2002) Crystallization and preliminary X-ray analysis of the membrane-bound cytochrome *c* nitrite reductase complex (NrfHA) from *Wolinella succinogenes*. *Acta Crystallogr. D Biol. Crystallogr.* **58,** 341–342
15. Reedy, C. J., and Gibney, B. R. (2004) Heme protein assemblies. *Chem. Rev.* **104,** 617–649
16. Martinez, S. E., Huang, D., Ponomarev, M., Cramer, W. A., and Smith, J. L. (1996) The heme redox center of chloroplast cytochrome *f* is linked to a buried five-water chain. *Protein Sci.* **5,** 1081–1092
17. Einsle, O., Messerschmidt, A., Stach, P., Bourenkov, G. P., Bartunik, H. D., Huber, R., and Kroneck, P. M. (1999) Structure of cytochrome *c* nitrite reductase. *Nature* **400,** 476–480
18. Rodrigues, M. L., Oliveira, T. F., Pereira, I. A., and Archer, M. (2006) X-ray structure of the membrane-bound cytochrome c quinol dehydrogenase NrfH reveals novel haem coordination. *EMBO J.* **25,** 5951–5960
19. Leys, D., Backers, K., Meyer, T. E., Hagen, W. R., Cusanovich, M. A., and Van Beeumen, J. J. (2000) Crystal structures of an oxygen-binding cytochrome *c* from *Rhodobacter sphaeroides*. *J. Biol. Chem.* **275,** 16050–16056
20. Cheesman, M. R., Little, P. J., and Berks, B. C. (2001) Novel heme ligation in a *c*-type cytochrome involved in thiosulfate oxidation: EPR and MCD of SoxAX from *Rhodovulum sulfidophilum*. *Biochemistry* **40,** 10562–10569
21. Bamford, V. A., Berks, B. C., and Hemmings, A. M. (2002) Novel domain packing in the crystal structure of a thiosulphate-oxidizing enzyme. *Biochem. Soc. Trans.* **30,** 638–642
22. Grein, F., Venceslau, S. S., Schneider, L., Hildebrandt, P., Todorovic, S., Pereira, I. A. C., and Dahl, C. (2010) DsrJ, an essential part of the DsrMKJOP complex in the purple sulfur bacterium *Allochromatium vinosum*, is an unusual triheme cytochrome *c*. *Biochemistry* **49,** 8290–8299
23. Pires, R. H., Venceslau, S. S., Morais, F., Teixeira, M., Xavier, A. V., and Pereira, I. A. C. (2006) Characterization of the *Desulfovibrio desulfuricans* ATCC 27774 DsrMKJOP complex: a membrane-bound redox complex involved in the sulfate respiratory pathway. *Biochemistry* **45,** 249–262
24. Van Driessche, G., Devreese, B., Fitch, J. C., Meyer, T. E., Cusanovich, M. A., and Van Beeumen, J. J. (2006) GHP, a new *c*-type green heme protein from *Halochromatium salexigens* and other proteobacteria. *FEBS J.* **273,** 2801–2811
25. Alric, J., Tsukatani, Y., Yoshida, M., Matsuura, K., Shimada, K., Hienerwadel, R., Schoepp-Cothenet, B., Nitschke, W., Nagashima, K. V. P., and Verméglio, A. (2004) Structural and functional characterization of the unusual triheme cytochrome bound to the reaction center of *Rhodovulum sulfidophilum*. *J. Biol. Chem.* **279,** 26090–26097
26. Suga, M., Lai, T.-L., Sugiura, M., Shen, J.-R., and Boussac, A. (2013) Crystal structure at 1.5 Å resolution of the PsbV2 cytochrome from the cyanobacterium *Thermosynechococcus elongatus*. *FEBS Lett.* **587,** 3267–3272
27. Blattner, F. R., Williams, B. G., Blechl, A. E., Denniston-Thompson, K., Faber, H. E., Furlong, L., Grunwald, D. J., Kiefer, D. O., Moore, D. D., Schumm, J. W., Sheldon, E. L., and Smithies, O. (1977) Charon phages: safer derivatives of bacteriophage λ for DNA cloning. *Science* **196,** 161–169
28. Ausubel, F. A., Brent, R., Kingston, R. E., Moore, D. D., Seidman, J. G., Smith, J. A., and Struhl, K. (1997) Media preparation and bacteriological tools. In *Current Protocols in Molecular Biology*, John Wiley & Sons, Inc., New York
29. Dahl, C., Schulte, A., Stockdreher, Y., Hong, C., Grimm, F., Sander, J., Kim, R., Kim, S.-H., and Shin, D. H. (2008) Structural and molecular genetic insight into a wide-spread bacterial sulfur oxidation pathway. *J. Mol. Biol.* **384,** 1287–1300
30. Pott, A. S., and Dahl, C. (1998) Sirohaem-sulfite reductase and other proteins encoded in the *dsr* locus of *Chromatium vinosum* are involved in the oxidation of intracellular sulfur. *Microbiology* **144,** 1881–1894
31. Horton, R. M. (1995) PCR mediated recombination and mutagenesis: SOEing together tailor-made genes. *Mol. Biotechnol.* **3,** 93–99
32. Brito, J. A., Gutierres, A., Denkmann, K., Dahl, C., and Archer, M. (2014) Production, crystallization and preliminary crystallographic analysis of *Allochromatium vinosum* TsdA, an unusual acidophilic *c*-type cytochrome. *Acta Crystallogr. F Struct. Biol. Commun.* **70,** 1424–1427
33. Dahl, C., Engels, S., Pott-Sperling, A. S., Schulte, A., Sander, J., Lübbe, Y., Deuster, O., and Brune, D. C. (2005) Novel genes of the *dsr* gene cluster and evidence for close interaction of Dsr proteins during sulfur oxidation in the phototrophic sulfur bacterium *Allochromatium vinosum*. *J. Bacteriol.* **187,** 1392–1404
34. Thomas, P. E., Ryan, D., and Levin, W. (1976) Improved staining procedure for detection of peroxidase-activity of cytochrome P-450 on sodium

dodecyl-sulfate polyacrylamide gels. *Anal. Biochem.* **75,** 168–176
35. Zehnder, A. J. B., and Wuhrmann, K. (1976) Titanium(III) citrate as a nontoxic oxidation-reduction buffering system for culture of obligate anaerobes. *Science* **194,** 1165–1166
36. Kabsch, W. (2010) XDS. *Acta Crystallogr. D Biol. Crystallogr.* **66,** 125–132
37. Terwilliger, T. C., Adams, P. D., Read, R. J., McCoy, A. J., Moriarty, N. W., Grosse-Kunstleve, R. W., Afonine, P. V., Zwart, P. H., and Hung, L. W. (2009) Decision-making in structure solution using Bayesian estimates of map quality: the PHENIX AutoSol wizard. *Acta Crystallogr. D Biol. Crystallogr.* **65,** 582–601
38. Terwilliger, T. C. (2003) Statistical density modification using local pattern matching. *Acta Crystallogr. D Biol. Crystallogr.* **59,** 1688–1701
39. Terwilliger, T. C., Grosse-Kunstleve, R. W., Afonine, P. V., Moriarty, N. W., Zwart, P. H., Hung, L. W., Read, R. J., and Adams, P. D. (2008) Iterative model building, structure refinement and density modification with the PHENIX AutoBuild wizard. *Acta Crystallogr. D Biol. Crystallogr.* **64,** 61–69
40. Emsley, P., Lohkamp, B., Scott, W. G., and Cowtan, K. (2010) Features and development of Coot. *Acta Crystallogr. D Biol. Crystallogr.* **66,** 486–501
41. Afonine, P. V., Grosse-Kunstleve, R. W., Echols, N., Headd, J. J., Moriarty, N. W., Mustyakimov, M., Terwilliger, T. C., Urzhumtsev, A., Zwart, P. H., and Adams, P. D. (2012) Towards automated crystallographic structure refinement with phenix.refine. *Acta Crystallogr. D Biol. Crystallogr.* **68,** 352–367
42. Lovell, S. C., Davis, I. W., Arendall, W. B., 3rd, de Bakker, P. I., Word, J. M., Prisant, M. G., Richardson, J. S., and Richardson, D. C. (2003) Structure validation by Cα geometry: ϕ,ψ and Cβ deviation. *Proteins* **50,** 437–450
43. Chen, V. B., Arendall, W. B., 3rd, Headd, J. J., Keedy, D. A., Immormino, R. M., Kapral, G. J., Murray, L. W., Richardson, J. S., and Richardson, D. C. (2010) MolProbity: all-atom structure validation for macromolecular crystallography. *Acta Crystallogr. D Biol. Crystallogr.* **66,** 12–21
44. Blanc, E., Roversi, P., Vonrhein, C., Flensburg, C., Lea, S. M., and Bricogne, G. (2004) Refinement of severely incomplete structures with maximum likelihood in BUSTER-TNT. *Acta Crystallogr. D Biol. Crystallogr.* **60,** 2210–2221
45. DeLano, W. L. (2013) *The PyMOL Molecular Graphics System*, version 1.5.0.4, Schrödinger, LLC, New York
46. Matthews, B. W. (1968) Solvent content of protein crystals. *J. Mol. Biol.* **33,** 491–497
47. Holm, L., and Rosenström, P. (2010) Dali server: conservation mapping in 3D. *Nucleic Acids Res.* **38,** W545–W549
48. Page, C. C., Moser, C. C., Chen, X., and Dutton, P. L. (1999) Natural engineering principles of electron tunneling in biological oxidation-reduction. *Nature* **402,** 47–52
49. Pereira, I. A. C., and Xavier, A. V. (2005) in *Encyclopedia of Inorganic and Bioinorganic Chemistry*, Vol. 5 (King, R. B., ed) pp. 3360–3376, John Wiley & Sons, Inc., New York
50. Dambe, T., Quentmeier, A., Rother, D., Friedrich, C., and Scheidig, A. J. (2005) Structure of the cytochrome complex SoxXA of *Paracoccus pantotrophus*, a heme enzyme initiating chemotrophic sulfur oxidation. *J. Struct. Biol.* **152,** 229–234
51. Marques, M. C., Coelho, R., Pereira, I. A. C., and Matias, P. M. (2014) Redox state-dependent changes in the crystal structure of [NiFeSe] hydrogenase from *Desulfovibrio vulgaris* Hildenborough. *Int. J. Hydr. Energ.* **38,** 8664–8682
52. Girvan, H. M., Seward, H. E., Toogood, H. S., Cheesman, M. R., Leys, D., and Munro, A. W. (2007) Structural and spectroscopic characterization of P450 BM3 mutants with unprecedented P450 heme iron ligand sets: new heme ligation states influence conformational equilibria in P450 BM3. *J. Biol. Chem.* **282,** 564–572
53. Miles, C. S., Manson, F. D. C., Reid, G. A., and Chapman, S. K. (1993) Substitution of a haem-iron axial ligand in flavocytochrome b_2. *Biochim. Biophys. Acta* **1202,** 82–86
54. Zhong, F., Lisi, G. P., Collins, D. P., Dawson, J. H., and Pletneva, E. V. (2014) Redox-dependent stability, protonation, and reactivity of cysteine-bound heme proteins. *Proc. Natl. Acad. Sci. U.S.A.* **111,** E306–E315
55. Marvin, K. A., Kerby, R. L., Youn, H., Roberts, G. P., and Burstyn, J. N. (2008) The transcription regulator RcoM-2 from *Burkholderia xenovorans* is a cysteine-ligated hemoprotein that undergoes a redox-mediated ligand switch. *Biochemistry* **47,** 9016–9028
56. Rother, D., and Friedrich, C. G. (2002) The cytochrome complex SoxXA of *Paracoccus pantotrophus* is produced in *Escherichia coli* and functional in the reconstituted sulfur-oxidizing enzyme system. *Biochim. Biophys. Acta* **1598,** 65–73
57. Bradley, J. M., Marritt, S. J., Kihlken, M. A., Haynes, K., Hemmings, A. M., Berks, B. C., Cheesman, M. R., and Butt, J. N. (2012) Redox and chemical activities of the hemes in the sulfur oxidation pathway enzyme SoxAX. *J. Biol. Chem.* **287,** 40350–40359
58. Reijerse, E. J., Sommerhalter, M., Hellwig, P., Quentmeier, A., Rother, D., Laurich, C., Bothe, E., Lubitz, W., and Friedrich, C. G. (2007) The unusal redox centers of SoxXA, a novel *c*-type heme-enzyme essential for chemotrophic sulfur-oxidation of *Paracoccus pantotrophus*. *Biochemistry* **46,** 7804–7810
59. Kappler, U., Bernhardt, P. V., Kilmartin, J., Riley, M. J., Teschner, J., McKenzie, K. J., and Hanson, G. R. (2008) SoxAX cytochromes, a new type of heme copper protein involved in bacterial energy generation from sulfur compounds. *J. Biol. Chem.* **283,** 22206–22214
60. Thauer, R. K., Jungermann, K., and Decker, K. (1977) Energy conservation in chemotrophic anaerobic bacteria. *Bacteriol. Rev.* **41,** 100–180
61. Kappler, U., Aguey-Zinsou, K.-F., Hanson, G. R., Bernhardt, P. V., and McEwan, A. G. (2004) Cytochrome *c*551 from *Starkeya novella*: characterization, spectroscopic properties, and phylogeny of a diheme protein of the SoxAX family. *J. Biol. Chem.* **279,** 6252–6260
62. Reedy, C. J., Elvekrog, M. M., and Gibney, B. R. (2008) Development of a heme protein structure electrochemical function database. *Nucleic Acids Res.* **36,** D307–D313
63. Williams, P. A., Fülöp, V., Garman, E. F., Saunders, N. F. W., Ferguson, S. J., and Hajdu, J. (1997) Haem-ligand switching during catalysis in crystals of a nitrogen-cycle enzyme. *Nature* **389,** 406–412
64. Fukumori, Y., and Yamanaka, T. (1979) A high-potential nonheme iron protein (HiPIP)-linked, thiosulfate-oxidizing enzyme derived from *Chromatium vinosum*. *Curr. Microbiol.* **3,** 117–120
65. Hanahan, D. (1983) Studies on transformation of *Escherichia coli* with plasmids. *J. Mol. Biol.* **166,** 557–580
66. Arslan, E., Schulz, H., Zufferey, R., Künzler, P., and Thöny-Meyer, L. (1998) Overproduction of *Bradyrhizobium japonicum c*-type cytochrome subunits of the cbb_3 oxidase in *Escherichia coli*. *Biochem. Biophys. Res. Commun.* **251,** 744–747
67. Karplus, P. A., and Diederichs, K. (2012) Linking crystallographic model and data quality. *Science* **336,** 1030–1033